Testing Brans-Dicke gravity using the Einstein telescope

Xing Zhang, Jiming Yu, Tan Liu, Wen Zhao, and Anzhong Wang

Phys. Rev. D **95**, 124008 — Published 6 June 2017

DOI: 10.1103/PhysRevD.95.124008

Testing Brans-Dicke gravity using Einstein Telescope

Xing Zhang,[1] Jiming Yu,[1] Tan Liu,[1] Wen Zhao,[1,*] and Anzhong Wang[2,3]

[1] *CAS Key Laboratory for Researches in Galaxies and Cosmology, Department of Astronomy, University of Science and Technology of China, Chinese Academy of Sciences, Hefei, Anhui 230026, China*

[2] *Institute for Advanced Physics and Mathematics, Zhejiang University of Technology, Hangzhou, Zhejiang 310032, China*

[3] *GCAP-CASPER, Department of Physics, Baylor University, Waco, Texas 76798-7316, USA*

Abstract

Gravitational radiation is an excellent field for testing theories of gravity in strong gravitational fields. The current observations on the gravitational-wave (GW) bursts by LIGO have already placed various constraints on the alternative theories of gravity. In this paper, we investigate the possible bounds which could be placed on the Brans-Dicke gravity using GW detection from inspiralling compact binaries with the proposed Einstein Telescope, a third-generation GW detector. We first calculate in details the waveforms of gravitational radiation in the lowest post-Newtonian approximation, including the tensor and scalar fields, which can be divided into the three polarization modes, i.e. "plus mode", "cross mode" and "breathing mode". Applying the stationary phase approximation, we obtain their Fourier transforms, and derive the correction terms in amplitude, phase and polarization of GWs, relative to the corresponding results in General Relativity. Imposing the noise level of Einstein Telescope, we find that the GW detection from inspiralling compact binaries, composed of a neutron star and a black hole, can place stringent constraints on the Brans-Dicke gravity. The bound on the coupling constant $\omega_{\rm BD}$ depends on the mass, sky-position, inclination angle, polarization angle, luminosity distance, redshift distribution and total observed number $N_{\rm GW}$ of the binary systems. Taking into account all the burst events up to redshift $z = 5$, we find that the bound could be $\omega_{\rm BD} \gtrsim 10^6 \times (N_{\rm GW}/10^4)^{1/2}$. Even for the conservative estimation with 10^4 observed events, the bound is still more than one order tighter than the current limit from solar system experiments. So, we conclude that Einstein Telescope will provide a powerful platform to test alternative theories of gravity.

PACS numbers: 98.70.Vc, 98.80.Cq, 04.30.-w

*wzhao7@ustc.edu.cn

I. INTRODUCTION

Since Einstein's General Relativity (GR) was proposed more than 100 years ago, a large number of experimental tests have been performed on various scales, from submillimeter scales tests in the laboratory, to the tests in solar system and cosmological scales [1–5]. Even so, most of these efforts have focused on the gravitational effects in weak fields. Different from them, gravitational radiation provides an excellent opportunity to experimentally test gravitational theories in the strong field regime. Since the observed gravitational waves (GWs) are always produced in either strong gravitational fields, extremely high energy scales, or the very early Universe, and are nearly freely propagating in the spacetime once generated, they encodes the clean information of these extreme conditions. Thus, a huge attention has been devoted to the detection of GWs. On September 14, 2015, the first direct GW signal, GW150914, was observed by LIGO, which marks the beginning of the era of GW astronomy [6]. Since then, various investigations on testing GR, including those from LIGO collaborations, have been carried out by utilizing the observed GW data [6–9].

Karl Popper argued that scientists can never truly "prove" that a theory, including GR, is correct, but rather all we do is to disprove, or more accurately to constrain a hypothesis. The theory that remains and cannot be disproved by observations becomes the *status quo* [10]. According to this argument, in order to test GR we much compare its predictions with alternative theories of gravity. So, the theoretical studies on gravitational radiations in various theories are highly desirable. For instance, in the previous work [11], the authors developed the parameterized post-Einsteinian (ppE) framework to describe the modifications of GWs in a wide class of gravitational theories.

In this paper, we will focus on Brans-Dicke (BD) gravity. As the simplest scalar-tensor gravity, BD gravity has been well studied and constrained in various tests (see for instance [12, 13]). For the gravitational radiation of inspiralling compact binaries in BD gravity, Will et al. have calculated the gravitational waveforms by including the lowest order effects [1, 14, 15][1]. Similar calculations have also applied to some extended versions of BD gravity [20–24]. However, for the gravitational waveforms, in these works the authors have only considered the phase correction terms in the "plus-mode" and "cross-mode" of GWs. As well-known, for the compact systems, the predictions of gravitational radiation in BD gravity are different from those in GR in several aspects [1]: First, modifications of the effective masses of the bodies, parameterized by the sensitivities s_i, alter the motion of two-body orbits, which induces the modification on the time dependence of the orbital frequency and GW frequency of the system. Second, in addition to the quadrupole gravitational radiation, in BD gravity the scalar field also emits scalar radiations, including the monopole, dipole and quadrupole components. These radiations also modify the orbital evolution of the system and thence the GW frequency and amplitude. In this paper, we extend the previous calculations on the gravitational radiation of compact binary system in BD gravity, and derive the full waveforms of GWs by including the "plus mode", "cross mode" as well as the "breathing mode". Employing the stationary phase approximation, we obtain the Fourier transforms of these components, and find that the contribution of scalar monopole radiation is negligible, and the dipole and quadrupole scalar radiations are suppressed by the BD parameter $\omega_{\rm BD}$ and/or the difference in sensitivities of two objects. The tensor quadrupole radiations are modified in both GW phases and amplitudes, which are significant in the low frequency range.

It is well-known that BD gravity reduces to GR in the limit $\omega_{\rm BD} \to \infty$. Many effects have been devoted to constrain the parameter $\omega_{\rm BD}$ in various systems [1, 12, 13]. Until now, the most stringent constraint is $\omega_{\rm BD} > 4 \times 10^4$, which comes from the Cassini-Huygens experiment [25]. In the previous work [14], the authors showed that observations of inspiral binary systems from ground-based detectors of the type of the advanced LIGO could place a bound of $\omega_{\rm BD} \gtrsim 2000$. If considering the LISA space interferometer, for a neutron star inspiralling into a $10^3\ M_\odot$ black hole in the Virgo Cluster, a possible bound of $\omega_{\rm BD} \gtrsim 3\times 10^5$ could be placed in a two-year integration [26, 27]. Similar results are also derived in the previous works [28, 29]. In addition, if considering the observations of potential space-based DICEGO/BBO projects, the bound $\omega_{\rm BD} \gtrsim 4 \times 10^8$ could be placed in the far future [30]. In this paper, we shall apply similar analyses to the potential observations of Einstein Telescope (ET). Currently, ET is undergoing a design study as a third-generation ground-based GW observatory [31], which would be able to observe binary neutron star systems up to redshift $z \sim 2$ and the neutron-star/black-hole events up to $z \sim 8$. Comparing with the generation of the advanced LIGO, which is often referred to as the second generation, ET has the following advantages: The noise power spectral density (PSD) of ET will be more than two orders smaller, while the lower cutoff frequency of ET will extend to 1 Hz. Both factors will greatly improve the total number of inspiralling compact binaries, as well as the signal-to-noise ratio for the given target. So, we anticipate that BD gravity can be well constrained by the potential observations of ET. In the previous works [32, 33], the authors found that, if considering ET, one GW event could place a bound of $\omega_{\rm BD} \gtrsim (10^4 \sim 10^5)$. In this paper, we shall extend these analyses by combining multiple events, and

[1] These calculations have been extended to the higher post-Newtonian (PN) orders in the recent works [16–19].

considering all the modifications of GW waveforms.

The outline of this paper is as follows. In Sec. II we calculate the gravitational waveforms of compact binary systems in BD gravity, derive their Fourier transforms by applying the stationary phase approximation, and then extend them to include high PN terms. In Sec. III, we discuss the capabilities of ET on constraining BD gravity by taking into account a large number of GW events in a wide redshift range. In Sec. IV we conclude the paper with a summary of our main results.

Throughout this paper, the signatures of metric are chosen as $(-,+,+,+)$, and the Greek indices $(\mu,\nu,\cdots)$ run over $0,1,2,3$. We choose the units in which $G=c=1$, where G is the Newtonian gravitational constant, and c is the speed of light in vacuum.

II. GRAVITATIONAL RADIATIONS IN SCALAR-TENSOR GRAVITY

A. BD gravity

In the Jordan frame, the action of the general scalar-tensor gravity is given by [1]

$$I=\frac{1}{16\pi}\int\left[\phi R-\frac{\omega(\phi)}{\phi}g^{\mu\nu}\phi_{,\mu}\phi_{,\nu}+2\phi\lambda(\phi)\right]\sqrt{-g}d^4x+I_m(g_{\mu\nu},q_A), \tag{1}$$

where $g_{\mu\nu}$ is the spacetime metric, g is its determinant, R is the Ricci scalar derived from this metric, ϕ is the scalar field, and $\omega(\phi)$ is the scalar-tensor coupling function, $\lambda(\phi)$ is the cosmological function. I_m represents the matter action, which depends only on the matter fields q_A and the metric $g_{\mu\nu}$, i.e. there is no direct interaction with the scalar field. In this paper, we restrict our attention to the massless BD theory, in which $\omega(\phi)=\omega_{\rm BD}$ is a constant, and $\lambda(\phi)=0$.

The field equations derived from the action of BD gravity are given by

$$R_{\mu\nu}-\frac{1}{2}g_{\mu\nu}R=\frac{8\pi}{\phi}T_{\mu\nu}+\frac{\omega_{\rm BD}}{\phi^2}\left(\phi_{,\mu}\phi_{,\nu}-\frac{1}{2}g_{\mu\nu}\phi_{,\rho}\phi^{,\rho}\right)+\frac{1}{\phi}(\phi_{;\mu\nu}-g_{\mu\nu}\Box_g\phi), \tag{2}$$

$$\Box_g\phi=\frac{1}{3+2\omega_{\rm BD}}\left(8\pi T-16\pi\phi\frac{\partial T}{\partial\phi}\right), \tag{3}$$

where $T_{\mu\nu}$ is the stress-energy tensor of matter and nongravitational fields, and $T\equiv g^{\alpha\beta}T_{\alpha\beta}$ is its trace. Throughout this paper, we use commas to denote ordinary derivatives, semicolons to denote covariant derivatives, and $\Box_g\equiv g^{\alpha\beta}\nabla_\alpha\nabla_\beta$ to represent the d'Alembertian with indices raised by the metric $g^{\mu\nu}$. Here, we should mention that in the general Jordan frame, the quantity $\partial T/\partial\phi$ is not present. But for the gravitationally bound bodies, as to be shown below, it will be present in the field equations.

In order to discuss the gravitational radiation, we assume that far away from the sources, the metric $g_{\mu\nu}$ reduces to the Minkowski metric $\eta_{\mu\nu}$, and the scalar field ϕ tends to its cosmological value ϕ_0. Thus, we can define the perturbations in the far-zone as follows,

$$h_{\mu\nu}=g_{\mu\nu}-\eta_{\mu\nu},\quad \varphi=\phi-\phi_0, \tag{4}$$

$$\theta^{\mu\nu}=h^{\mu\nu}-\frac{1}{2}h\eta^{\mu\nu}-(\varphi/\phi_0)\eta^{\mu\nu}, \tag{5}$$

where φ is the perturbation of the scalar field ϕ about its asymptotic cosmological value ϕ_0. Note that in another version of the field equations [16, 34], an auxiliary metric $\tilde{g}_{\mu\nu}$ is introduced, which relates to the physical metric $g_{\mu\nu}$ by the conformal transformation $\tilde{g}_{\mu\nu}\equiv(\phi/\phi_0)g_{\mu\nu}$, and a "gothic" version of this metric, $\tilde{\mathfrak{g}}^{\mu\nu}\equiv\sqrt{-\tilde{g}}\tilde{g}^{\mu\nu}$. In the weak field approximations, it can be proved that $\theta^{\mu\nu}=\eta^{\mu\nu}-\tilde{\mathfrak{g}}^{\mu\nu}$. Following the previous works [1, 14, 15], in this paper we shall use the quantities $\theta^{\mu\nu}$ and φ. Choosing the harmonic gauge in which $\theta^{\mu\nu}_{\ \ ,\nu}=0$, we can rewrite the field equations for BD theory in the form

$$\Box_\eta\theta^{\mu\nu}=-16\pi\tau^{\mu\nu},\quad \Box_\eta\varphi=-8\pi\tau_s, \tag{6}$$

where the sources terms $\tau^{\mu\nu}$ and τ_s are explicitly given in [15, 16, 34], and $\tau^{\mu\nu}$ satisfies the conservation laws $\tau^{\mu\nu}_{\ \ ,\nu}=0$ because of the Bianchi identity. Note that the indices of $\theta^{\mu\nu}$ and $\varphi_{,\mu}$ will be lowered and raised by $\eta_{\mu\nu}$ and $\eta^{\mu\nu}$.

B. Evolution of binary systems in BD gravity

Now, let us turn to consider a realistic source, which is made of two compact objects. Since the compact system is gravitationally bound, its total mass depends on its internal gravitational energy, which in turn depends on the effective local value of the scalar field ϕ in the vicinity of the body. Eardley found that these effects could be accounted for by simply replacing the constant inertial mass of the object in the distributional stress-energy tensor of the "crude" approach by a function of the scalar field ϕ, namely $m_i(\phi)$ $(i = 1, 2)$ [35]. Thus, the matter action in Eq. (1) becomes

$$I_m = -\sum_{i=1,2} \int m_i(\phi) d\tau_i, \tag{7}$$

where τ_i denotes the proper time along the trajectory of the object i. These modifications depend on the internal structure of the bodies and the theory of gravity. We expand $m_i(\phi)$ about the asymptotic value ϕ_0 as follows,

$$m_i(\phi) = m_i \left[1 + s_i \left(\frac{\phi}{\phi_0} \right) + \frac{1}{2}(s_i^2 + s_i' - s_i) \left(\frac{\phi}{\phi_0} \right)^2 + O\left(\frac{\phi}{\phi_0} \right)^3 \right], \tag{8}$$

where $m_i \equiv m_i(\phi_0)$, and the sensitivity s_i and its derivative s_i' are defined as

$$s_i \equiv \left(\frac{d \ln m_i(\phi)}{d \ln \phi} \right)_{\phi=\phi_0}, \quad s_i' \equiv \left(\frac{d^2 \ln m_i(\phi)}{d(\ln \phi)^2} \right)_{\phi=\phi_0}. \tag{9}$$

The sensitivities s_i roughly measure the gravitational binding energy per unit mass. This effect violates the Strong Equivalence Principle, in the sense that the motion of such bodies now depends on their internal structure (apart from tidal interactions). In BD gravity, for white dwarfs we have $s \simeq 0$, for neutron stars $s \approx 0.1 - 0.2$ [15], and for black holes $s = 0.5$ [36].

The stress-energy tensor in this system is given by

$$T^{\mu\nu} = (-g)^{-1/2} \sum_{i=1,2} m_i(\phi) u_i^\mu u_i^\nu (u_i^0)^{-1} \delta^3(\mathbf{x} - \mathbf{x}_i), \tag{10}$$

$$\frac{\partial T}{\partial \phi} = -(-g)^{-1/2} \sum_{i=1,2} \frac{\partial m_i(\phi)}{\partial \phi} (u_i^0)^{-1} \delta^3(\mathbf{x} - \mathbf{x}_i), \tag{11}$$

where u_i^μ is the four-velocity of the object i.

In this system, we treat the objects as point-like, with masses m_1 and m_2, and positions $\mathbf{x_1}$ and $\mathbf{x_2}$, respectively. From the post-Newtonian equations of motion [1], in the center-of-mass frame, it was shown that the dynamics in the Newtonian limit reduces to a one-body system with a mass equal to the reduced mass $\mu = m_1 m_2/(m_1 + m_2)$, and the equation of motion [15]

$$d^2\mathbf{x}/dt^2 = -\mathcal{G} m \mathbf{x}/r^3, \tag{12}$$

where $m = m_1 + m_2$ is the total mass and $\mathbf{x} = \mathbf{x_2} - \mathbf{x_1}$ the relative coordinate. The parameter $\mathcal{G}$ is defined as,

$$\mathcal{G} = 1 - \xi(s_1 + s_2 - 2 s_1 s_2), \quad \xi = (2 + \omega_{\rm BD})^{-1}. \tag{13}$$

In this paper, we consider only the case of quasi-circular orbits (that is, circular, apart from an adiabatic inspiral). Then the orbital frequency ω_s is related to the orbital radius r by $v^2 = \mathcal{G}m/r$ with the orbital velocity $v = \omega_s r$. So, we have Kepler's third law

$$\omega_s = (\mathcal{G}m/r^3)^{1/2}, \tag{14}$$

and the orbit period P_s is given by $P_s = 2\pi/\omega_s$. The energy of the system is given by

$$E = -(1/2)\mathcal{G}\mu m/r. \tag{15}$$

For a compact binary system, the dissipation of its total energy is caused by the emission of gravitational radiations. In BD gravity, the rate of energy loss for a quasi-circular two-body orbit is given by [1, 15]

$$\frac{dE}{dt} = -\left\langle \frac{8}{15} \frac{\mu^2 m^2}{r^4} (12\kappa v^2 + \frac{5}{8} \kappa_D \mathcal{S}^2) \right\rangle, \tag{16}$$

where the angular brackets denote an orbital average, and the coefficients are given by

$$\kappa = \mathcal{G}^2(1 - \frac{1}{2}\xi + \frac{1}{12}\xi\Gamma^2), \quad \kappa_D = 2\mathcal{G}^2\xi, \quad \mathcal{S} = s_1 - s_2, \quad \Gamma = 1 - 2(m_1 s_2 + m_2 s_1)/m. \tag{17}$$

The first term in Eq. (16) represents the combined effects of the quadrupole and monopole radiations, and the second term is the contribution of the dipole radiation. If $\kappa \to 1$ and $\kappa_D \to 0$, it reduces to that of GR.

C. Gravitational waveforms in BD gravity

The gravitational radiations can be derived by solving the wave equations of Eq. (6). For a binary orbit, to leading order of $v^2 \sim m/r$, the solutions of the spatial components of the perturbations are given by [1, 15],

$$\theta^{ij} = 2(1-\xi/2){d_{\rm L}}^{-1}(d^2/dt^2)\sum_{k=1,2} m_k(\phi)x_k^i x_k^j = (4\mu/d_{\rm L})(1-\xi/2)(v^i v^j - \mathcal{G}m x^i x^j/r^3), \tag{18}$$

$$\varphi/\phi_0 = \xi(\mu/d_{\rm L})\left\{\Gamma[(\hat{\mathbf{N}}\cdot\mathbf{v})^2 - \mathcal{G}m(\hat{\mathbf{N}}\cdot\mathbf{x})^2/r^3] - (\mathcal{G}\Gamma + 2\Lambda)m/r - 2\mathcal{S}(\hat{\mathbf{N}}\cdot\mathbf{v})\right\}, \tag{19}$$

where the parameter Λ is given by $\Lambda = 1 - s_1 - s_2$, $d_{\rm L}$ is the luminosity distance of the observer, and $\hat{\mathbf{N}}$ is the direction unit vector of $d_{\rm L}$. In the flat Friedmann-Lemaître-Robertson-Walker universe, the luminosity distance is calculate by [37]

$$d_{\rm L}(z) = (1+z)\int_0^z \frac{dz'}{H(z')}, \tag{20}$$

where z is the redshift, and $H(z)$ is the Hubble parameter. In the spatial flat ΛCDM model, it is given by

$$H(z) = H_0[\Omega_m(1+z)^3 + \Omega_\Lambda]^{1/2}. \tag{21}$$

Throughout this paper, we adopt a fiducial cosmological model with the following values of the parameters [38]:

$$\Omega_m = 0.314, \quad \Omega_\Lambda = 0.686, \quad \Omega_k = 0, \quad H_0 = 67.3\text{km s}^{-1}\text{Mpc}^{-1}. \tag{22}$$

The perturbation of the metric is obtained by utilizing the relation [2]

$$h^{\mu\nu} = \theta^{\mu\nu} - \eta^{\mu\nu}\theta/2 - (\varphi/\phi_0)\eta^{\mu\nu}. \tag{23}$$

A gravitational-wave detector measures the separation ξ^i between the two test masses. If the distance between them is small compared to the wavelength of GWs, and the test masses move slowly, the separation obeys the equation $d^2\xi^i/dt^2 = -R^{0i0j}\xi^j$ [39]. The components of the Riemann tensor R^{0i0j} measured by a detector can be shown to be given by [39, 40]

$$R^{0i0j} = \frac{1}{2}(\partial^i\partial^0 h^{0j} + \partial^j\partial^0 h^{0i} - \partial^0\partial^0 h^{ij} - \partial^i\partial^j h^{00}) \equiv -\frac{1}{2}\frac{d^2}{dt^2}\mathrm{h}^{ij}, \tag{24}$$

where we have defined the effective gravitational waveform h^{ij}. Using Eq. (23) and the relation $\partial^i(\varphi/\phi_0) = -\partial_0(\varphi/\phi_0)\hat{N}^i$, we derive that

$$\mathrm{h}^{ij} = \theta^{ij}_{\rm TT} - (\varphi/\phi_0)(\delta^{ij} - \hat{N}^i\hat{N}^j), \tag{25}$$

where TT denotes the transverse-traceless projection. Note that the full gravitational waveform is transverse but not traceless because of the presence of the scalar contribution in Eq. (25). For quasi-circular orbits, by employing the relation $v^2 = \mathcal{G}m/r$, the waveform of Eq. (25) becomes [14, 16] [3]

$$\mathrm{h}^{ij} = \frac{2\mu}{d_{\rm L}}\left[Q^{ij}_{TT} + S(\delta^{ij} - \hat{N}^i\hat{N}^j)\right], \tag{26}$$

---

[2] There is a typo in the formulae (2.7) of Ref. [14], where $\bar{h}^{ij}$ should be replaced by h^{ij}.
[3] There is a typo in the formulae (2.9) and (2.10c) of Ref. [14], and the similar typo also appears in Eq. (41) of Ref. [41].

$$Q^{ij} = 2(1-\frac{1}{2}\xi)\frac{\mathcal{G}m}{r}(\hat{\lambda}^i\hat{\lambda}^j - \hat{n}^i\hat{n}^j), \tag{27}$$

$$S = -\frac{1}{2}\xi\left\{\frac{\Gamma\mathcal{G}m}{r}[(\hat{\mathbf{N}}\cdot\hat{\lambda})^2 - (\hat{\mathbf{N}}\cdot\hat{\mathbf{n}})^2] - (\mathcal{G}\Gamma+2\Lambda)\frac{m}{r} - 2\mathcal{S}(\frac{\mathcal{G}m}{r})^{1/2}\hat{\mathbf{N}}\cdot\hat{\lambda}\right\}, \tag{28}$$

where we have defined the unit vectors $\hat{\mathbf{n}} \equiv \mathbf{x}/r$ and $\hat{\lambda} \equiv \mathbf{v}/v$.

In metric theories of gravity, up to six degrees of freedom are allowed [1]. In addtion to the "plus mode" (denoted as $+$, the real part of the Weyl tensor component Ψ_4) and "cross mode" (denoted as $\times$, the imaginary part of the Weyl tensor component Ψ_4), they include a scalar "breathing mode" (denoted as b, the traceless part of the Ricci tensor, Φ_{22}), a scalar longitudinal mode (denoted as L, the Weyl tensor component Ψ_2), and two vectorial modes (denoted as x and y, the real and imaginary parts of the Weyl tensor component Ψ_3, respectively). So, in general, the full (effective) metric perturbations take the form

$$\mathrm{h}_{ij} = h_+\mathrm{e}^+_{ij} + h_\times\mathrm{e}^\times_{ij} + h_b\mathrm{e}^b_{ij} + h_L\mathrm{e}^L_{ij} + h_x\mathrm{e}^x_{ij} + h_y\mathrm{e}^y_{ij}, \tag{29}$$

where the polarization tensors are defined as

$$\mathrm{e}^+_{ij} = \hat{e}_x\otimes\hat{e}_x - \hat{e}_y\otimes\hat{e}_y, \quad \mathrm{e}^\times_{ij} = \hat{e}_x\otimes\hat{e}_y + \hat{e}_y\otimes\hat{e}_x, \tag{30}$$

$$\mathrm{e}^b_{ij} = \hat{e}_x\otimes\hat{e}_x + \hat{e}_y\otimes\hat{e}_y, \quad \mathrm{e}^L_{ij} = \hat{e}_z\otimes\hat{e}_z, \tag{31}$$

$$\mathrm{e}^x_{ij} = \hat{e}_x\otimes\hat{e}_z + \hat{e}_z\otimes\hat{e}_x, \quad \mathrm{e}^y_{ij} = \hat{e}_y\otimes\hat{e}_z + \hat{e}_z\otimes\hat{e}_y. \tag{32}$$

In the E(2) classification for GWs, the massless scalar-tensor theories (including BD gravity) are of Class N_3, i.e. the nonzero components are h_+, $h_\times$ and h_b [1]. In Appendix A, we proved that the first term of h^{ij} in Eq. (26) corresponds to the "plus" and "cross" polarization modes of the GWs. From Eq. (26), we observe that these two terms are given by

$$h_+(t) = -\frac{4\mathcal{G}\mu m}{d_\mathrm{L} r}(1-\frac{1}{2}\xi)\frac{1+\cos^2\iota}{2}\cos 2\Phi(t), \tag{33}$$

$$h_\times(t) = -\frac{4\mathcal{G}\mu m}{d_\mathrm{L} r}(1-\frac{1}{2}\xi)\cos\iota\sin 2\Phi(t), \tag{34}$$

where ι is the inclination angle of the binary orbital angular momentum along the line of sight. The polarization angle is calculated by $\Phi(t) = \int_{t_0}^{t}\omega_s(t')dt' + \Phi_0$, where Φ_0 is the initial phase at $t = t_0$. In BD gravity, from the relation of (14), we have

$$\frac{\mu m}{r} = M_c^{5/3}(2\pi f_s)^{2/3}\mathcal{G}^{-1/3}, \tag{35}$$

where $M_c = \mu^{3/5}m^{2/5}$ is the chirp mass. Thus, these two components can be rewritten as

$$h_+(t) = -\frac{4\beta}{d_\mathrm{L}}M_c^{5/3}(2\pi f_s)^{2/3}\frac{1+\cos^2\iota}{2}\cos 2\Phi(t), \tag{36}$$

$$h_\times(t) = -\frac{4\beta}{d_\mathrm{L}}M_c^{5/3}(2\pi f_s)^{2/3}\cos\iota\sin 2\Phi(t), \tag{37}$$

where $\beta \equiv (1-\frac{1}{2}\xi)\mathcal{G}^{2/3}$ is the correction factor in BD gravity. In the case $\beta = 1$, these results reduce to those of GR [40].

The second term in Eq. (26) exactly corresponds to the breathing mode of GWs, which can be written as the sum of three terms,

$$h_b(t) = \frac{2\mu}{d_\mathrm{L}}S \equiv h_{b1} + h_{b2} + h_{b3}, \tag{38}$$

where

$$h_{b1}(t) = -\frac{\mu m}{d_\mathrm{L} r}(\xi\Gamma\mathcal{G})\sin^2\iota\cos 2\Phi(t), \quad h_{b2}(t) = \frac{\mu m}{d_\mathrm{L} r}(\mathcal{G}\Gamma+2\Lambda), \quad h_{b3}(t) = \frac{2\mu}{d_\mathrm{L}}(\xi\mathcal{S})(\mathcal{G}m/r)^{1/2}\sin\iota\cos\Phi(t). \tag{39}$$

Using the relation (14), they can be rewritten as

$$h_{b1}(t) = -\frac{\xi\Gamma\mathcal{G}}{d_{\rm L}} M_c^{5/3}(2\pi f_s)^{2/3}\mathcal{G}^{-1/3}\sin^2\iota\cos 2\Phi(t), \tag{40}$$

$$h_{b2}(t) = \frac{\mathcal{G}\Gamma+2\Lambda}{d_{\rm L}} M_c^{5/3}(2\pi f_s)^{2/3}\mathcal{G}^{-1/3}, \tag{41}$$

$$h_{b3}(t) = \frac{2\xi\mathcal{S}}{d_{\rm L}} M_c^{5/3}(2\pi f_s/m)^{1/3}\sin\iota\cos\Phi(t). \tag{42}$$

D. Waveforms in the stationary phase approximation

To compute the Fisher information matrix we would need the Fourier transform $\tilde{h}(f)$ of the signal $h(t)$. During the inspiral, the change in orbital frequency over a single period is negligible, and it is possible to apply a stationary phase approximation (SPA) to compute the Fourier transformation. Given a function $B(A) = 2A(t)\cos\phi(t)$, where $d\ln A/dt \ll d\phi(t)/dt$ and $|d^2\phi/dt^2| \ll (d\phi/dt)^2$, the SPA provides the following estimate of the Fourier transform $\tilde{B}(f)$ (see, for instance, [40]):

$$\tilde{B}(f) \simeq \frac{A(t_f)}{\sqrt{\dot{F}(t_f)}} e^{i[\Psi_f(t_*)-\pi/4]}, \quad f \geq 0, \tag{43}$$

where $\Psi_f(t) \equiv 2\pi f t - \phi(t)$, $2\pi F(t) \equiv d\phi/dt$. In this equation t_* is defined as the time at which $F(t_*) = f$ and $\Psi_f(t_*)$ is the value of $\Psi_f(t)$ at $t = t_*$. We first calculate the evolution of the frequency $f_s \equiv w_s/2\pi$ in BD gravity. From the evolution equations (12), (14) and (16), we derive that

$$\dot{f}_s = \frac{48\mu\mathcal{G}^{1/2}}{5\pi m^3}\left(\frac{m}{r}\right)^{11/2}\left(\kappa + \frac{5}{96}\frac{\kappa_D}{\mathcal{G}}\frac{r}{m}\mathcal{S}^2\right), \tag{44}$$

from which we find that

$$(2\pi\mathcal{M}_c f_s)^{-8/3}[1-(4/5)b\eta^{2/5}(2\pi\mathcal{M}_c f_s)^{-2/3}] = (256/5)(t_c-t)/\mathcal{M}_c, \tag{45}$$

where $\eta \equiv \mu/m$ is the symmetric mass ratio, t_c is the time at which $f_s \to \infty$. We have defined the quantities,

$$\mathcal{M}_c \equiv (\kappa^{3/5}/\mathcal{G}^{4/5})\eta^{3/5}m, \quad b \equiv (5/96)(\kappa^{-3/5}\mathcal{G}^{-6/5})\kappa_D\mathcal{S}^2. \tag{46}$$

In the case $\kappa \to 1$ and $\mathcal{G} \to 1$, we find that $\mathcal{M}_c$ reduces to the chirp mass M_c. In BD gravity with $\xi \ll 1$ (i.e. $\omega_{\rm BD} \gg 1$) and $\mathcal{S} \lesssim 1$, we always have $b \ll 1$. Taking into account the fact that [14]

$$z \equiv b\eta^{2/5}(2\pi\mathcal{M}_c f_s)^{-2/3} \leq 5\times 10^{-3}\left(\frac{500}{\omega_{\rm BD}}\right)\left(\frac{\mathcal{S}}{0.5}\right)^2\left(\frac{M_\odot}{\mathcal{M}_c}\right)\left(\frac{30{\rm Hz}}{f_s}\right)^{2/3}, \tag{47}$$

up to the first order of z, we obtain the relation between f_s and t,

$$\omega_s = 2\pi f_s = \frac{1}{\mathcal{M}_c}\left(\frac{256(t_c-t)}{5\mathcal{M}_c}\right)^{-3/8}\left[1-\frac{3}{10}b\eta^{2/5}\left(\frac{256(t_c-t)}{5\mathcal{M}_c}\right)^{1/4}\right]. \tag{48}$$

Now, let us focus on the Fourier transformation of the "plus mode" by utilizing the result (36). Since the amplitude varies slowly in comparison with the phase $2\Phi(t)$, the stationary point $t_*(f)$ is determined by the condition $2\pi f = 2\dot{\Phi}(t_*) = 4\pi f_s(t_*)$, i.e. $f = 2f_s(t_*)$, which expresses the fact that the largest contribution to the Fourier component $\tilde{h}_+(f)$ with a given f is obtained for the value of t such that the chirping frequency f is equal to $2f_s$. Using the relations given in (43) and (48), and from (36) we derive that

$$\tilde{h}_+(f) = \sqrt{\frac{5}{24}}\frac{1}{\pi^{2/3}}\frac{1}{d_{\rm L}}M_c^{5/6}f^{-7/6}\frac{1+\cos^2_\iota}{2}(-\beta)\left[1-\frac{1}{2}b\eta^{2/5}(\pi\mathcal{M}_c f)^{-2/3}\right]\kappa^{-1/2}\mathcal{G}^{2/3}e^{i\Psi_+(f)}, \tag{49}$$

where the phase is given by

$$\Psi_+(f) = -2\psi_c + 2\pi f t_c - \frac{\pi}{4} + \frac{3}{128}(\pi\mathcal{M}_c f)^{-5/3}\left[1-\frac{4}{7}b\eta^{2/5}(\pi\mathcal{M}_c f)^{-2/3}\right], \tag{50}$$

where ψ_c is the phase of binary system at time t_c. The expression of the phase is consistent with that given in [14].

Following a similar procedure, we can derive the Fourier components for the "cross" and "breathing" modes, which are given by

$$\tilde{h}_\times(f) = \sqrt{\frac{5}{24}}\frac{1}{\pi^{2/3}}\frac{1}{d_{\rm L}}M_c^{5/6}f^{-7/6}\cos\iota(-\beta)\left[1-\frac{1}{2}b\eta^{2/5}(\pi\mathcal{M}_c f)^{-2/3}\right]\kappa^{-1/2}\mathcal{G}^{2/3}e^{i\Psi_\times(f)}, \tag{51}$$

$$\tilde{h}_{b1}(f) = \sqrt{\frac{5}{24}}\frac{1}{\pi^{2/3}}\frac{1}{d_{\rm L}}M_c^{5/6}f^{-7/6}\sin^2\iota(-\xi\Gamma/4)\left[1-\frac{1}{2}b\eta^{2/5}(\pi\mathcal{M}_c f)^{-2/3}\right]\kappa^{-1/2}\mathcal{G}^{4/3}e^{i\Psi_+(f)}, \tag{52}$$

$$\tilde{h}_{b3}(f) = \sqrt{\frac{5}{48}}\frac{1}{\pi^{2/3}}\frac{1}{d_{\rm L}}M_c^{5/6}(2f)^{-7/6}\sin\iota(2\pi mf)^{-1/3}\kappa^{-1/2}\mathcal{G}\xi\mathcal{S}\left[1-\frac{1}{2}b\eta^{2/5}(2\pi\mathcal{M}_c f)^{-2/3}\right]e^{i\Psi_{b3}(f)}, \tag{53}$$

where the phases are

$$\Psi_\times(f) = \Psi_+(f)+\frac{\pi}{2}, \tag{54}$$

$$\Psi_{b3}(f) = -\psi_c+2\pi ft_c-\frac{\pi}{4}+\frac{3}{256}(2\pi\mathcal{M}_c f)^{-5/3}\left[1-\frac{4}{7}b\eta^{2/5}(2\pi\mathcal{M}_c f)^{-2/3}\right]. \tag{55}$$

Let us turn to the h_{b2} component. From Eq. (41), we know that the phase is zero, and the value of $h_{b2}(t)$ depending on time t is only through slowly varying function $f_s(t)$. So, the Fourier component $\tilde{h}_{b2}(f)$ is negligible in comparison with the other terms.

In order to extend these results easily to high post-Newtonian orders, we rewrite the expressions of h_+ and $h_\times$ in the forms,

$$h_+(t)=\frac{2\beta\eta mx}{d_{\rm L}}H_+^{(0)},\quad h_\times(t)=\frac{2\beta\eta mx}{d_{\rm L}}H_\times^{(0)}, \tag{56}$$

where

$$x=(2\pi mf_s)^{2/3},\quad H_+^{(0)}=-(1+\cos^2\iota)\cos2\Phi(t),\quad H_\times^{(0)}=-2\cos\iota\sin2\Phi(t). \tag{57}$$

A detector measures only a certain linear combination of the GW components, called the response $h(t)$. For BD gravity, it is given by

$$h(t)=F_+(\theta,\phi,\psi)h_+(t)+F_\times(\theta,\phi,\psi)h_\times(t)+F_b(\theta,\phi,\psi)h_b(t), \tag{58}$$

where F_+, $F_\times$ and F_b are the detector antenna pattern functions, ψ is the polarization angle as mentioned above, (θ,ϕ) are angles describing the location of source on the sky, relative to the detector. In general these angles are time-dependent. In the case of Einstein Telescope, considered in this paper, compact binary systems can be in band for hours, but almost all of the signal-to-noise ratio will be accumulated only at the final minutes of the inspiral process. In the sequel, (θ,ϕ,ψ) will be considered as constants [4].

The Fourier component of $h(t)$ becomes,

$$\tilde{h}(f)=F_+\tilde{h}_+(f)+F_\times\tilde{h}_\times(f)+F_b[\tilde{h}_{b1}(f)+\tilde{h}_{b3}(f)]\equiv\tilde{h}^{(1)}(f)+\tilde{h}^{(2)}(f), \tag{59}$$

where

$$\begin{aligned}\tilde{h}^{(1)}(f) &= \frac{M_c^{5/6}}{d_{\rm L}}\sqrt{\frac{5}{48}}\pi^{-2/3}(2f)^{-7/6}\left\{E(2\pi mf)^{-1/3}+ES_{-1}(2\pi mf)^{-1}\right\}\\ &\quad\times\Theta(f_{\rm LSO}-f)\exp[i(2\pi ft_c-\pi/4+\psi(f))],\end{aligned} \tag{60}$$

$$\begin{aligned}\tilde{h}^{(2)}(f) &= 2^{-1/2}\frac{M_c^{5/6}}{d_{\rm L}}\sqrt{\frac{5}{48}}\pi^{-2/3}f^{-7/6}\left\{[Qe^{-i\varphi_{(2,0)}}P_{(2,0)}+A]S_{-1}(\pi mf)^{-2/3}+[Qe^{-i\varphi_{(2,0)}}P_{(2,0)}+A]\right\}\\ &\quad\times\Theta(2f_{\rm LSO}-f)\exp[i(2\pi ft_c-\pi/4+2\psi(f/2))],\end{aligned} \tag{61}$$

[4] Note that with LISA, Doppler modulation due to the orbital motion, as well as spin precession, will allow for accurate determination of the angular parameters (see, for instance, [42] and references therein), but this is unlikely to happen for BNS (or NSBH) signals in ET with Doppler modulation due to the Earth's rotation. Nevertheless, some improvement in parameter estimation can be expected, which for simplicity we do not take into account here.

in which $\Theta(x)$ is the usual Heaviside function, $P_{(2,0)}$ and $\varphi_{(2,0)}$ are defined in Appendix B. The upper cutoff frequency is dictated by the last stable orbit of the binary system, which marks the end of the inspiral regime and the onset of the finial merge. We assume that this occurs when the radiation frequency reaches $f = kf_{\rm LSO}$ for the k-th harmonic, with $f_{\rm LSO} = 1/(6^{3/2}2\pi m)$ being the orbital frequency at the last stable orbit [5]. Note that, for the sources at cosmological distances, what enters the waveform is the *observed* mass, which differs from the *physical* mass by a factor $(1+z)$: $m_{\rm obs} = (1+z)m_{\rm phys}$ [40]. Throughout this paper, all the masses refer to the observed quantity if there is no special instruction. In these expressions, we have defined the following coefficients to characterize the modifications of BD gravity,

$$E = \kappa^{-1/2}\mathcal{G}\sin\iota F_b\xi\mathcal{S}, \quad A = -\frac{1}{2}\xi\Gamma\sin^2\iota F_b\kappa^{-1/2}\mathcal{G}^{4/3}, \quad Q = (1-\frac{1}{2}\xi)\kappa^{-1/2}\mathcal{G}^{4/3}, \quad S_{-1} = -\frac{1}{2}b\kappa^{-2/5}\mathcal{G}^{8/15}. \tag{62}$$

The uniform phase function $\psi(f)$ is given by

$$\psi(f) = -\psi_c + \frac{3}{256(2\pi\mathcal{M}_c f)^{5/3}}\sum_{i=-2}^{0}\psi_i(2\pi m f)^{i/3} \tag{63}$$

with

$$\psi_{-2} = -\frac{4}{7}b\kappa^{-2/5}\mathcal{G}^{8/15}, \quad \psi_{-1} = 0, \quad \psi_0 = 1. \tag{64}$$

The quantity Q describes the modifications on the amplitudes of the "plus" and "cross" modes. In addition, A, E, S_{-1} and Q together describe the extra "breathing" mode, which is absent in GR. The modification of the phase is described by ψ_{-2}. In the case with $E \to 0$, $A \to 0$, $S_{-1} \to 0$, $\psi_{-2} \to 0$, $Q \to 1$ and $\mathcal{M}_c \to M_c$, the expression of $\tilde{h}(f)$ reduces to that of GR. Expressions of Eqs. (60), (61) and (63) show that, in comparison with the waveform given in GR, the corrections of BD gravity are mainly at the low frequency range. Since the coefficients E, S_{-1} and ψ_{-2} all directly depend on the difference in sensitivities $\mathcal{S}$, the corrections caused by the related terms vanish for the binary neutron star systems (if assuming the sensitivities of neutron stars are the same), as well as for binary black hole systems. In addition, for the binary black hole systems with $s_i = 0.5$, we have $\Gamma = 0$, and the coefficient A and its related terms also vanish. So, in comparison with GR, the difference of the gravitational waveforms from BD gravity is very small. For these reasons, in this paper, we shall only use the compact binary systems that are composed of a neutron star and a black hole, in order to constrain BD gravity.

E. Extension to high post-Newtonian orders

In GR and alternative theories of gravity, the gravitational waveforms should include high-order PN terms to construct the real templates for the GW detectors. In the PN approximations of GR, the waveforms are expressed as expansions in terms of the orbital velocity v, and have been developed by many authors (see [43] and references therein). For the non-spinning compact objects, the best waveforms currently available are of 2.5 PN order in amplitude [44] and 3.5 PN order in phase [45]. In the scalar-tensor gravity, the equations of motion for non-spinning compact objects have been developed to 2.5 PN order [18], and the tensor and scalar gravitational waveforms have also been calculated up to 2 and 1.5 PN order, respectively [16, 17].

In this subsection, we shall extend the waveforms and their Fourier components in BD gravity derived above to high-order PN approximations, in which the waveforms are linear combinations of harmonics in the orbital phase, and the k-th harmonics is cutoff at $kf_{\rm LSO}$ in the frequency domain. Including the higher PN orders in waveforms, in particular in terms of orbital phase, the corrections could significantly alter the signal-to-noise ratio of the GW sources [46]. Different from the previous works [16, 17], we consider only the leading order corrections of waveforms (including polarization mode, amplitude and phase) caused by BD gravity in comparison with GR, and add these correction terms to the high PN waveforms of GR. Since the BD parameter $\omega_{\rm BD}$ has been tightly constrained by various experiments, the correction terms of the gravitational waveforms in BD gravity are expected to be very small. And the corrections from higher PN orders are expected to be even smaller than the leading-order ones.

---

[5] Note that, there is a small mistake in Eq. (41) in Ref. [41], where the coefficient of $-\frac{1}{4}\xi$ should be replaced by $-\frac{1}{2}\xi$. If taking into account this mistake, the formulae in (60) and (61) are consistent with the expressions of Eq. (55) and (54) in Ref. [41].

In the stationary phase approximation, the amplitude-corrected waveforms in GR is explicitly presented in [46], in which the total Fourier component $\tilde{h}(f)$ is the sum of seven harmonics, i.e.

$$\tilde{h}(f) = \sum_{k=1}^{7} \tilde{h}^{(k)}(f). \tag{65}$$

Taking into account the corrections caused by BD gravity in comparison with GR, the expressions of harmonics $\tilde{h}^{(k)}(f)$ are revised to the following forms,

$$\begin{aligned}
\tilde{h}^{(1)}(f) &= \frac{M_c^{5/6}}{d_{\rm L}}\sqrt{\frac{5}{48}}\pi^{-2/3}(2f)^{-7/6}\Big\{ES_{-1}(2\pi mf)^{-1}+E(2\pi mf)^{-1/3}\\
&+e^{-i\varphi_{(1,1/2)}}P_{(1,1/2)}(2\pi mf)^{1/3}\\
&+\left[e^{-i\varphi_{(1,3/2)}}P_{(1,3/2)}+e^{-i\varphi_{(1,1/2)}}P_{(1,1/2)}S_1\right](2\pi mf)\\
&+\left[e^{-i\varphi_{(1,2)}}P_{(1,2)}+e^{-i\varphi_{(1,1/2)}}P_{(1,1/2)}S_{3/2}\right](2\pi mf)^{4/3}\\
&+\left[e^{-i\varphi_{(1,5/2)}}P_{(1,5/2)}+e^{-i\varphi_{(1,3/2)}}P_{(1,3/2)}S_1+e^{-i\varphi_{(1,1/2)}}P_{(1,1/2)}S_2\right](2\pi mf)^{5/3}\Big\}\\
&\times\Theta(f_{\rm LSO}-f)\exp[i(2\pi ft_c-\pi/4+\psi(f))],\\
\tilde{h}^{(2)}(f) &= 2^{-1/2}\frac{M_c^{5/6}}{d_{\rm L}}\sqrt{\frac{5}{48}}\pi^{-2/3}f^{-7/6}\Big\{\left[A+Qe^{-i\varphi_{(2,0)}}\right]S_{-1}(\pi mf)^{-2/3}\\
&+\left[A+Qe^{-i\varphi_{(2,0)}}P_{(2,0)}\right]\\
&+\left[e^{-i\varphi_{(2,1)}}P_{(2,1)}+e^{-i\varphi_{(2,0)}}P_{(2,0)}S_1\right](\pi mf)^{2/3}\\
&+\left[e^{-i\varphi_{(2,3/2)}}P_{(2,3/2)}+e^{-i\varphi_{(2,0)}}P_{(2,0)}S_{3/2}\right](\pi mf)\\
&+\left[e^{-i\varphi_{(2,2)}}P_{(2,2)}+e^{-i\varphi_{(2,1)}}P_{(2,1)}S_1+e^{-\varphi_{(2,0)}}P_{(2,0)S_2}\right](\pi mf)^{4/3}\\
&+\left[e^{-i\varphi_{(2,5/2)}}P_{(2,5/2)}+e^{-i\varphi_{(2,3/2)}}P_{(2,3/2)}S_1+e^{-i\varphi_{(2,1)}}P_{(2,1)}S_{3/2}+e^{-i\varphi_{(2,0)}}P_{(2,0)}S_{5/2}\right](\pi mf)^{5/3}\Big\}\\
&\times\Theta(2f_{\rm LSO}-f)\exp[i(2\pi ft_c-\pi/4+2\psi(f/2))],\\
\tilde{h}^{(3)}(f) &= 3^{-1/2}\frac{M_c^{5/6}}{d_{\rm L}}\sqrt{\frac{5}{48}}\pi^{-2/3}(2f/3)^{-7/6}\Big\{e^{-i\varphi_{(3,1/2)}}P_{(3,1/2)}(2\pi mf/3)^{1/3}\\
&+\left[e^{-i\varphi_{(3,3/2)}}P_{(3,3/2)}+e^{-i\varphi_{(3,1/2)}}P_{(3,1/2)}S_1\right](2\pi mf/3)\\
&+\left[e^{-i\varphi_{(3,2)}}P_{(3,2)}+e^{-i\varphi_{(3,1/2)}}P_{(3,1/2)}S_{3/2}\right](2\pi mf/3)^{4/3}\\
&+\left[e^{-i\varphi_{(3,3/2)}}P_{(3,3/2)}S_1+e^{-i\varphi_{(3,1/2)}}P_{(3,1/2)}S_2\right](2\pi mf/3)^{5/3}\Big\}\\
&\times\Theta(3f_{\rm LSO}-f)\exp[i(2\pi ft_c-\pi/4+3\psi(f/3))],\\
\tilde{h}^{(4)}(f) &= 4^{-1/2}\frac{M_c^{5/6}}{d_{\rm L}}\sqrt{\frac{5}{48}}\pi^{-2/3}(f/2)^{-7/6}\Big\{e^{-i\varphi_{(4,1)}}P_{(4,1)}(\pi mf/2)^{2/3}\\
&+\left[e^{-i\varphi_{(4,2)}}P_{(4,2)}+e^{-i\varphi_{(4,1)}}P_{(4,1)}S_1\right](\pi mf/2)^{4/3}\\
&+\left[e^{-i\varphi_{(4,5/2)}}P_{(4,5/2)}+e^{-i\varphi_{(4,1)}}P_{(4,1)}S_{3/2}\right](\pi mf/2)^{5/3}\Big\}\\
&\times\Theta(4f_{\rm LSO}-f)\exp[i(2\pi ft_c-\pi/4+4\psi(f/4))],\\
\tilde{h}^{(5)}(f) &= 5^{-1/2}\frac{M_c^{5/6}}{d_{\rm L}}\sqrt{\frac{5}{48}}\pi^{-2/3}(2f/5)^{-7/6}\left\{e^{-i\varphi_{(5,3/2)}}P_{(5,3/2)}(2\pi mf/5)\right.\\
&\left.+\left[e^{-i\varphi_{(5,5/2)}}P_{(5,5/2)}+e^{-i\varphi_{(5,3/2)}}P_{(5,3/2)}S_1\right](2\pi mf/5)^{5/3}\right\}\\
&\times\Theta(5f_{\rm LSO}-f)\exp[i(2\pi ft_c-\pi/4+5\psi(f/5))],\\
\tilde{h}^{(6)}(f) &= 6^{-1/2}\frac{M_c^{5/6}}{d_{\rm L}}\sqrt{\frac{5}{48}}\pi^{-2/3}(f/3)^{-7/6}e^{-i\varphi_{(6,2)}}P_{(6,2)}(\pi mf/3)^{4/3}\\
&\times\Theta(6f_{\rm LSO}-f)\exp[i(2\pi ft_c-\pi/4+6\psi(f/6))],\\
\tilde{h}^{(7)}(f) &= 7^{-1/2}\frac{M_c^{5/6}}{d_{\rm L}}\sqrt{\frac{5}{48}}\pi^{-2/3}(2f/7)^{-7/6}e^{-i\varphi_{(7,5/2)}}P_{(7,5/2)}(2\pi mf/7)^{5/3}\\
&\times\Theta(7f_{\rm LSO}-f)\exp[i(2\pi ft_c-\pi/4+7\psi(f/7))],
\end{aligned}$$

where $P_{(m,n)}$, $\varphi_{(m,n)}$, S_i ($i \geq 1$) are all given in Appendix B. The other parameters, including E, A, Q, S_{-1}, are defined by Eq. (62). In these expressions, the phase function $\psi(f)$ is given by

$$\psi(f) = -\psi_c + \frac{3}{256(2\pi\mathcal{M}_c f)^{5/3}} \sum_{i=-2}^{7} \psi_i (2\pi m f)^{i/3}, \tag{66}$$

where ψ_{-2} and ψ_{-1} are given by Eq. (64), and ψ_i ($i \geq 0$) are given in Appendix B.

From the expression of $\tilde{h}(f)$ we find that the corrections caused by BD gravity exist both in the amplitudes $\tilde{h}^i(f)$ ($i = 1, 2$) and the phase $\psi(f)$. In order to investigate which effect is dominant for a typical binary system, we plot the waveforms $\tilde{h}^i(f)$ ($i = 1, 2, 3$) and the difference between GR and BD gravity in Fig. 1. In this system, we choose the mass of the black hole as $m_1 = 10M_\odot$ with the sensitivity $s_1 = 0.5$, the mass of the neutron star as $m_2 = 1.4M_\odot$ with the sensitivity $s_2 = 0.2$, and the BD parameter as $\xi = 0.001$. Note that, this number of ξ has already been ruled out by the Cassini experiment [25], which was used here only for an illustrative purpose. The left panels show that the second harmonic is much larger than the other ones, which dominates the signal-to-noise ratio of the event. The middle panels show that the values of $|\tilde{h}^{(i)}_{\rm BD} - \tilde{h}^{(i)}_{\rm GR}|$ are comparable to those of $\tilde{h}^{(i)}_{\rm BD}$ or $\tilde{h}^{(i)}_{\rm GR}$ for any given frequency f, which indices that the correction effects are significant in the BD gravity with $\xi = 0.001$. However, if ignoring the correction effects in the phase terms and considering only the amplitudes of the waveforms, we find that the values of $||\tilde{h}^{(i)}_{\rm BD}| - |\tilde{h}^{(i)}_{\rm GR}||$ become much smaller than those of $|\tilde{h}^{(i)}_{\rm BD}|$ or $|\tilde{h}^{(i)}_{\rm GR}|$. So, we conclude that the dominant effects of BD gravity are caused by the modification in the phase terms, rather than in the amplitude terms, which is consistent with the arguments given in [14, 27]. From the expression of $\psi(f)$ in Eq. (66), we observe that the modification on the phase terms has two effects: The chirp mass M_c in the denominator is replaced by $\mathcal{M}_c$, and an extra term $\psi_{-2}(2\pi m f)^{-2/3}$. Compared with the phase given in GR, the first effect increases the value of $\psi(f)$, and the latter decreases it. From the right panel of Fig. 1, we find that, in the low frequency range $f < 1.5$Hz, the first effect is dominant, and in the high frequency range $f > 1.5$Hz, the latter is dominant.

III. TESTING BD GRAVITY USING EINSTEIN TELESCOPE

A. Einstein Telescope and the estimation of GW parameters

The gravitational waveforms depend not only on the parameters of the binary system, but also on the parameters of the theory concerned (For example, in BD gravity, it is $\omega_{\rm BD}$). By the matched-filter analysis of GW observations, one can determine all the parameters together. In this paper, we shall focus on the observation of GW sources by ET, a third-generation ground-based GW detector. Although the basic design of ET is still under discussions, one possibility is to have three interferometers with 60° opening angles and 10 km arm lengths, arranged in an equilateral triangle [31]. The corresponding antenna pattern functions of ET for different polarization modes of GWs are given in Appendix C. The scientific potentials of ET have been studied by many authors [47–59].

The performance of a GW detector is characterized by the one-side noise *power spectral density* $S_h(f)$ (PSD), which plays an important role in the signal analysis. We take the noise PSD of ET to be [47, 60]

$$S_h(f) = S_0 \left[x^{p_1} + a_1 x^{p_2} + a_2 \frac{1 + b_1 x + b_2 x^2 + b_3 x^3 + b_4 x^4 + b_5 x^5 + b_6 x^6}{1 + c_1 x + c_2 x^2 + c_3 x^3 + c_4 x^4} \right], \tag{67}$$

where $x \equiv f/f_0$ with $f_0 = 200$Hz, and $S_0 = 1.449 \times 10^{-52}\,{\rm Hz}^{-1}$. The other parameters are as follows:

$$\begin{aligned} & p_1 = -4.05, \quad p_2 = -0.69, \quad a_1 = 185.62, \quad a_2 = 232.56, \\ b_1 = 31.18, \quad & b_2 = -64.72, \quad b_3 = 52.24, \quad b_4 = -42.16, \quad b_5 = 10.17, \quad b_6 = 11.53 \\ & c_1 = 13.58, \quad c_2 = -36.46, \quad c_3 = 18.56, \quad c_4 = 27.43. \end{aligned} \tag{68}$$

For the purpose of data analysis, the noise PSD is assumed to be essentially infinite below a certain low cutoff frequency $f_{\rm lower}$ (see the review [61]). For ET we take this to be $f_{\rm lower} = 1$ Hz.

For any given binary system, the waveforms in Eq. (65) depend on nine system parameters $(M_c, \eta, t_c, \psi_c, \iota, \theta, \phi, \psi, d_{\rm L})$ and one gravity parameter ξ (or $\omega_{\rm BD}$). By maximizing the correlation between a template waveform that depends on a set of parameters p_i ($i = 1, 2, 3, \cdots$) and a measured signal, the matched filtering provides a natural way to estimate the parameters of the signal and their errors. With a given detector noise $S_h(f)$, we employ the Fisher matrix approach [62]. Comparing with the Markov chain Monte Carlo (MCMC) analysis, the Fisher information

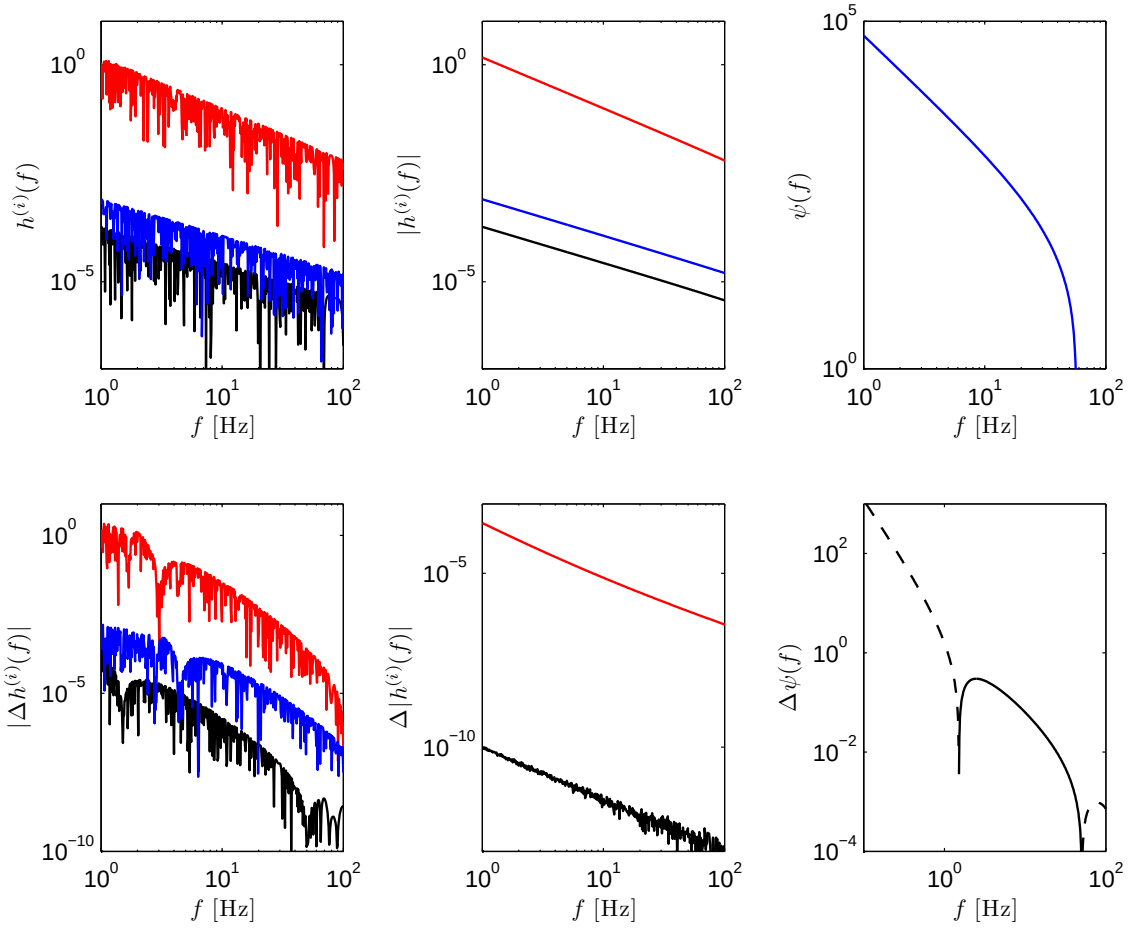

FIG. 1: Upper panels show the amplitudes and phase of the Fourier components $\tilde{h}^{(i)}(f)$ in BD gravity. Lower panels show $|\tilde{h}^{(i)}_{\rm BD} - \tilde{h}^{(i)}_{\rm GR}|$ (left), $||\tilde{h}^{(i)}_{\rm BD}| - |\tilde{h}^{(i)}_{\rm GR}||$ (middle) and $(\psi_{\rm BD} - \psi_{\rm GR})$ (right). In the left and middle panels, the black lines denote the results of the first harmonic with $i = 1$, the red lines are those with $i = 2$, and the blue lines are those with $i = 3$. In the right panels, the negative values of the function are depicted by the broken line. In this figure we have adopted the model with the parameters chosen as, $m_1 = 10M_\odot$, $m_2 = 1.4M_\odot$, $\theta = \phi = \psi = \iota = 0$, $\xi = 0.001$, $d_{\rm L} = 10^3$Mpc. Note that the units of the vertical axis in the left and middle panels are all rescaled by a factor $10^{-20}{\rm Hz}^{-1}$.

matrix analysis is simple and accurate enough to estimate the detection abilities of the future experiments. In the case of a single interferometer A ($A = 1, 2, 3$ for ET), the Fisher matrix is given by [14]

$$\Lambda^{\rm A}_{ij} = \langle \tilde{h}^{\rm A}_i(f), \tilde{h}^{\rm A}_j(f) \rangle, \quad \tilde{h}^{\rm A}_i(f) = \partial \tilde{h}^{\rm A}(f)/\partial p_i, \tag{69}$$

where $\tilde{h}^{\rm A}(f)$ is the output of the interferometer A, and p_i denote the free parameters to be estimated, which are

$$(M_c, \eta, t_c, \psi_c, \cos\iota, \cos\theta, \phi, \psi, \ln d_{\rm L}, \xi). \tag{70}$$

Note that, in this paper, we fix the sensitivities as follows: For neutron stars $s_2 = 0.2$, and for black holes $s_1 = 0.5$. The angular brackets denote the scalar product, which, for any two given functions $a(t)$ and $b(t)$, is defined as

$$\langle a, b \rangle = 4 \int_{f_{\rm lower}}^{f_{\rm upper}} \frac{\tilde{a}(f)\tilde{b}^*(f) + \tilde{a}^*(f)\tilde{b}(f)}{2} \frac{df}{S_h(f)}, \tag{71}$$

where $\tilde{a}$ and $\tilde{b}$ are the Fourier transforms of the functions $a(t)$ and $b(t)$. The Fisher matrix for the combination of the three independent interferometers is then

$$\Lambda_{ij} = \sum_{\rm A=1}^{3} \Lambda^{\rm A}_{ij}. \tag{72}$$

Once the total Fisher matrix Λ_{ij} is derived, an estimate of rms error, Δp_i, in measuring the parameter p_i can then be calculated in the limit of large signal-to-noise ratio, by taking the square root of the diagonal elements of the inverse of the Fisher matrix,

$$\Delta p_i = (\Sigma_{ii})^{1/2}, \quad \Sigma = \Lambda^{-1}. \tag{73}$$

The correlation coefficients between parameters p_i and p_j are given by

$$c_{ij} = \Sigma_{ij}/(\Sigma_{ii}\Sigma_{jj})^{1/2}. \tag{74}$$

Note that, in the limit case $c_{ij} = 0$ for any $i \neq j$, the error becomes $\Delta p_i \to (\Lambda_{ii})^{-1/2}$, which is also equivalent to the case in which all the other parameters, but p_i, are fixed at the parameter estimation.

The inner product also allows us to write the signal-to-noise ratios $\rho^{\rm A}$ $(A = 1, 2, 3)$ in a compact way:

$$\rho^{\rm A} = \sqrt{\langle \tilde{h}^{\rm A}(f), \tilde{h}^{\rm A}(f)\rangle}. \tag{75}$$

The combined signal-to-noise ratio for the network of the three independent interferometers is then

$$\rho = \left[\sum_{\rm A=1}^{3} \left(\rho^{\rm A}\right)^2\right]^{1/2}. \tag{76}$$

In Fig. 2, we plot the signal-to-noise ratio ρ for different compact binary systems at different positions, in which we find that the value of ρ strongly depends on the mass, the redshift, as well as their positions in the sky. For the given position, orbital and polarization angles, the higher redshift and/or the larger mass of the black hole follow the lower signal-to-noise ratio. If the sources are at the optimum position, $\theta = \psi = \iota = 0$, and the mass of the black hole is $m_{1,\rm phys} = 2M_\odot$, we have $\rho > 8$ for $z < 3.82$. If $m_{1,\rm phys} = 10M_\odot$, it becomes $\rho > 8$ so long as $z < 4.93$. In both cases, we find ET could detect the binary systems at very high redshifts. On the contrary, if the sources are at the position $\theta = \psi = \iota = \pi/2$, we have $\rho > 8$ for $z < 0.43$ and $m_{1,\rm phys} = 2M_\odot$, and $\rho > 8$ for $z < 0.70$ and $m_{1,\rm phys} = 10M_\odot$. In addition, from numerical calculations, we find that the signal-to-noise ratio ρ is independent of the position angle ϕ, which is determined by the equilateral triangle structure of ET.

In order to study the contribution of signal at each frequency band to the total signal-to-noise ratio ρ, we define the following quantity,

$$\mathcal{X}(f) \equiv \sum_{\rm A=1}^{3} \frac{4f(\Delta \ln f)|\tilde{h}^{\rm A}(f)|^2}{S_n(f)}, \tag{77}$$

where we bin the frequency band with $\Delta \ln(f/{\rm Hz}) = 0.001$ in this paper. It is obvious that $\mathcal{X}(f)$ at each frequency describes the relative contribution of the signal-to-noise ratio at this single frequency band f, and the total signal-to-noise ratio ρ^2 defined in Eq. (76) is the cumulative function of $\mathcal{X}(f)$ from $f = f_{\rm lower}$ to $f = f_{\rm upper}$. In Fig. 3 we plot the function $\mathcal{X}(f)$ and its cumulative function from $f_{\rm lower}$ to f for different objects. All the plots clearly show that the major contribution to the total ρ comes from the signal at the frequency range $f \in (30, 300)$Hz, which is caused by the fact that the noise PSD of ET is minimized about $f \sim 200$Hz.

B. Potential constraint on the parameter $\omega_{\rm BD}$ by ET

1. *Dependence on the mass of black hole*

As mentioned above, the corrections of the gravitational waveforms in BD gravity strongly depends on the difference in sensitivities $\mathcal{S}$, so we expect that only the compact binary systems including a neutron star and a black hole can well constrain the parameter $\omega_{\rm BD}$. So, in this paper, we shall only focus on this kind of systems. For the neutron star, we assume its physical mass is $m_{2,\rm phys} = 1.4M_\odot$ and the sensitivity parameter is $s_2 = 0.2$. For the black hole, we assume that its physical mass is in the range $m_{2,\rm phys} \in (2M_\odot, 100M_\odot)$, the sensitivity parameter is $s_1 = 0.5$, and the spin is zero.

Let us investigate what kind of systems can give a better constraint on the BD parameter. Let us first fix the following model parameters as $\theta = \phi = \psi = \iota = 0$, $t_c = \psi_c = 0$, $d_{\rm L} = 10^3$Mpc, $m_2 = 1.4M_\odot$, and $\xi = 0$ in the fiducial model. Then, we study the effect of m_1 on the value of $\Delta\xi$. Here, since $z \ll 1$, we ignore the difference between the

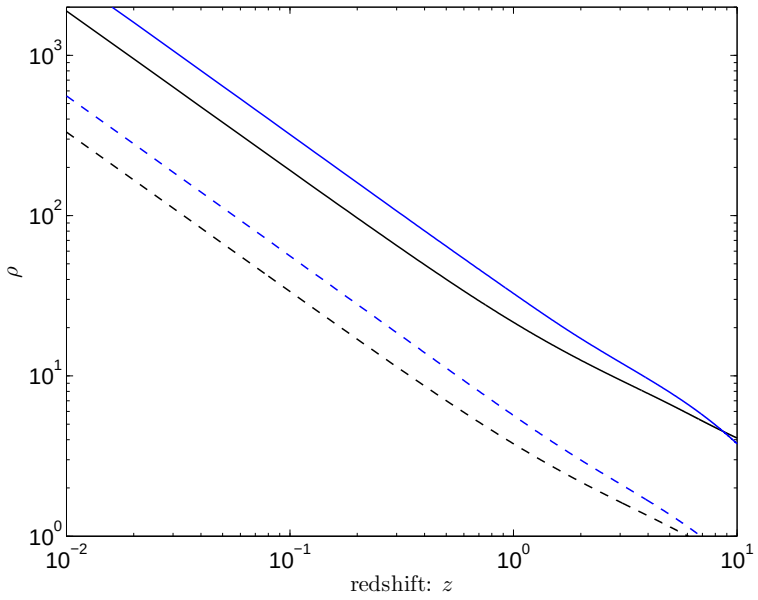

FIG. 2: Signal-to-noise ratio for the sources at different redshifts. The black solid line shows the result with the parameters $m_{1,\rm phys} = 2M_\odot$, $\theta = \phi = \psi = \iota = 0$; the blue solid line shows the results with $m_{1,\rm phys} = 10M_\odot$, $\theta = \phi = \psi = \iota = 0$. The black dashed line shows the result with the parameters $m_{1,\rm phys} = 2M_\odot$, $\theta = \phi = \psi = \iota = \pi/2$, and blue dashed line shows that with $m_{1,\rm phys} = 10M_\odot$, $\theta = \phi = \psi = \iota = \pi/2$. For the other parameters, in all cases we have adopted the same values: $t_c = 0$, $\psi_c = 0$, $\xi = 0.001$, $m_{2,\rm phys} = 1.4M_\odot$.

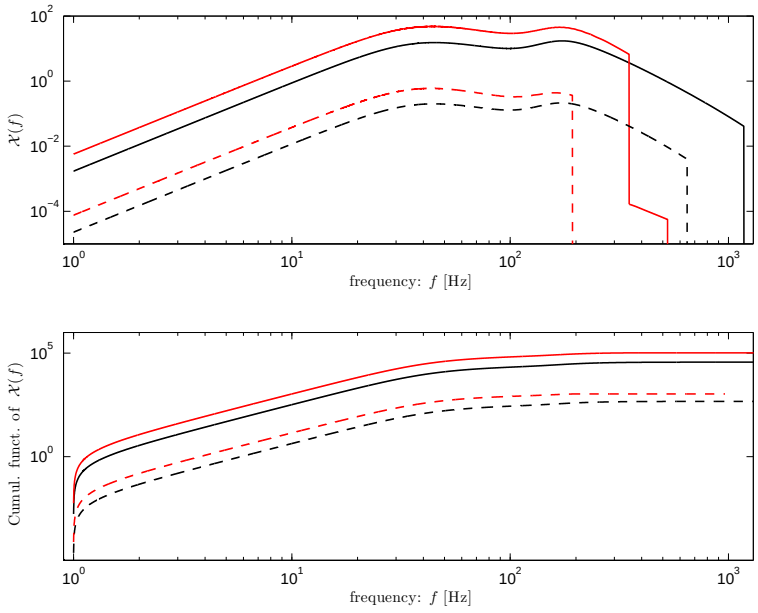

FIG. 3: The function $\mathcal{X}(f)$ for different frequencies f (upper panel), and its cumulative function from $f_{\rm lower}$ to f (lower panel). The black solid line shows the result with $m_{1,\rm phys} = 2M_\odot$ and $z = 0.1$, and the red solid line shows the result with $m_{1,\rm phys} = 10M_\odot$ and $z = 0.1$. The black dashed line shows the result with $m_{1,\rm phys} = 2M_\odot$ and $z = 1$, and the red dashed line shows the result with $m_{1,\rm phys} = 10M_\odot$ and $z = 1$. For the other parameters, in both cases we have set $\theta = \phi = \psi = \iota = 0$, $t_c = 0$, $\psi_c = 0$, $\xi = 0.001$, $m_{2,\rm phys} = 1.4M_\odot$.

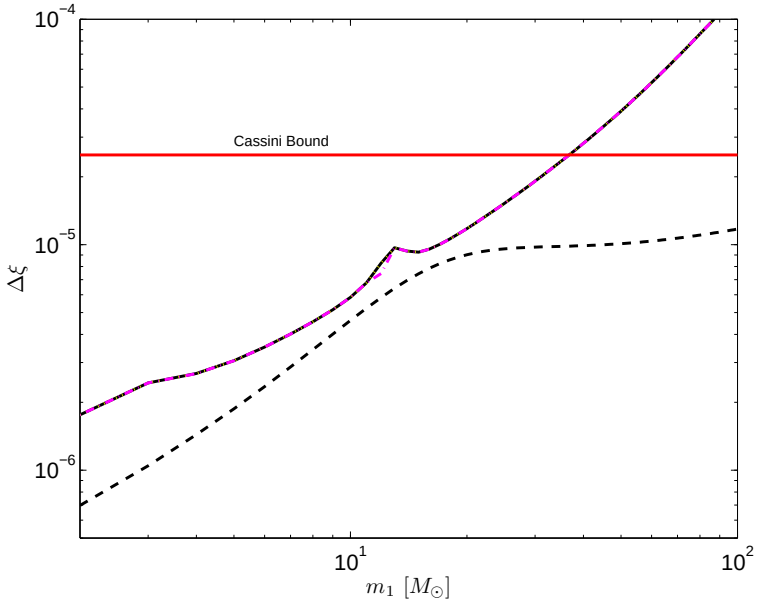

FIG. 4: The dependence of rms error $\Delta\xi$ on the black hole mass m_1. The other parameters in the fiducial model are set to $m_2 = 1.4M_\odot$, $t_c = 0$, $\psi_c = 0$, $\theta = \phi = \psi = \iota = 0$, $\xi = 0$, $d_{\rm L} = 10^3$Mpc. The black solid line shows the result in the case where all the ten parameters are set free. The black dashed line shows the result in the case where only ξ is set free. The yellow dashed line (which is overlapped with the black solid line) shows the result in the case where only the parameters $(M_c, \eta, t_c, \psi_c, \psi, \iota, \xi, \ln d_{\rm L})$ are set free. In the magenta dash-dotted line, we consider ten free parameters, but include only the phase correction in the gravitational waveforms. For comparison, we also plot the Cassini bound with red solid line.

observed masses m_i and the physical masses $m_{i,\rm phys}$. For each case, we solve the Fisher information matrix Λ_{ij} with ten free parameters, and derive the quantity $\Delta\xi$ by using the relation given in Eq. (73), which is plotted in Fig. 4, denoted by the black solid line. This figure clearly shows that a smaller mass m_1 of the black hole gives a lower value $\Delta\xi$, i.e. the more stringent constraint on the parameter $\omega_{\rm BD}$ is obtained. For the binary system with $m_1 = 2M_\odot$, we have $\Delta\xi = 1.76 \times 10^{-6}$, which is equivalent to the constraint $\omega_{\rm BD} > 0.57 \times 10^6$. However, if $m_1 = 100M_\odot$, the error of ξ becomes $\Delta\xi = 1.27 \times 10^{-4}$, i.e. $\omega_{\rm BD} > 0.79 \times 10^4$. As mentioned above, in this calculation, we have taken into account the correlation between ξ and the other parameters in the analysis. If considering the limit case, in which only the parameter ξ is set free, while all the other parameters are fixed, then we calculate the errors $\Delta\xi = \Lambda_{\xi\xi}^{-1/2}$ for different m_1, which is also plotted in Fig. 4, denoted by the black dashed line. Comparing it with the black solid line, we find that the results in these two cases are quite different, which shows that the cross-correlations between ξ and other parameters can significantly weaken the constraints on ξ. However, in both cases, the tendencies between $\Delta\xi$ and m_1 are the same, which are different from the results of signal-to-noise ratio ρ ploted in Fig. 2.

The Fisher matrix component $\Lambda_{\xi\xi}$ describes the sensitivity of ET on the parameter ξ (which is equivalent to $\omega_{\rm BD}$). In order to quantify the contribution of each frequency band to the total $\Lambda_{\xi\xi}$, we define the following quantity,

$$\mathcal{Y}(f) \equiv \sum_{\rm A=1}^{3} \frac{4f(\Delta \ln f)|\partial\tilde{h}^{\rm A}(f)/\partial\xi|^2}{S_n(f)} \tag{78}$$

where we bin the frequency band with $\Delta \ln(f/{\rm Hz}) = 0.001$ in this paper. The Fisher matrix component $\Lambda_{\xi\xi}$ defined in Eq. (72) is the cumulative function of $\mathcal{Y}(f)$ from $f = f_{\rm lower}$ to $f = f_{\rm upper}$. In Fig. 5 we plot the function $\mathcal{Y}(f)$ and its cumulative function from $f_{\rm lower}$ to f for various objects. Different from the results given in Fig. 3, the plots clearly show that the main contribution to the total $\Lambda_{\xi\xi}$ comes from the signal at the lowest frequency range $f \sim f_{\rm lower}$, which is understandable since the waveform difference between BD gravity and GR is mainly at the low frequency range. If increasing the mass of the black hole m_1, the frequency, in which the waveform difference is significant, will become lower. Thus, in the sensitive frequency band $f > 1$Hz of ET, the effect of BD gravity become weaker, which explains why a large m_1 gives rise to a weaker constraint on the parameter ξ.

In Section II, we know that the waveform correction caused by BD gravity can be divided into two parts: One is the correction in the phase term $\psi(f)$, and the other is in the amplitudes of $\tilde{h}^{(1)}(f)$ and $\tilde{h}^{(2)}(f)$. In the previous

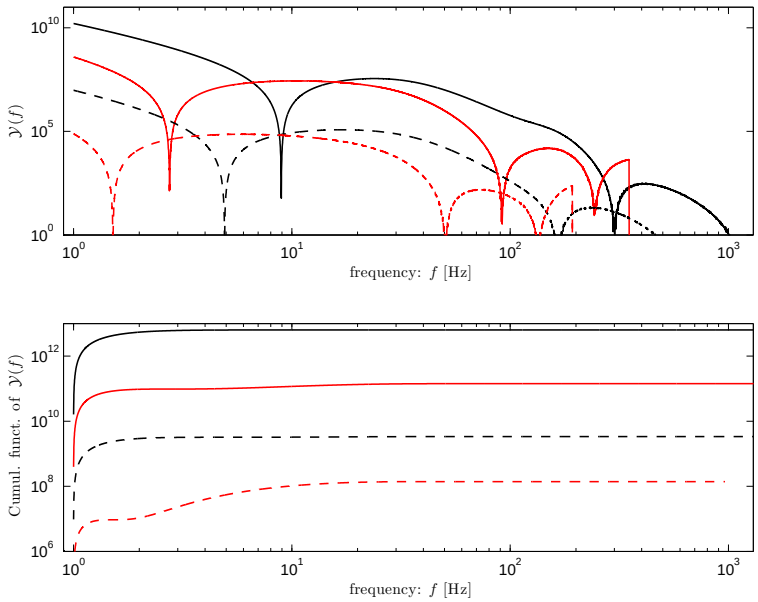

FIG. 5: The function $\mathcal{Y}(f)$ for different frequency f (upper panel), and its cumulative function from $f_{\rm lower}$ to f (lower panel). The black solid line shows the result with $m_{1,\rm phys} = 2M_\odot$ and $z = 0.1$, and the red solid line shows the result with $m_{1,\rm phys} = 10M_\odot$ and $z = 0.1$. The black dashed line shows the result with $m_{1,\rm phys} = 2M_\odot$ and $z = 1$, and the red dashed line shows the result with $m_{1,\rm phys} = 10M_\odot$ and $z = 1$. For the other parameters, in all cases we have set $\theta = \phi = \psi = \iota = 0$, $m_{2,\rm phys} = 1.4M_\odot$.

works [14, 27], the authors have only considered the correction in the phase term. Here, we will investigate how the corrections of the amplitudes can influence the value of $\Delta\xi$. In Fig. 4, we plot the rms error $\Delta\xi$ (the magenta line) in which only phase corrections are considered. We find that the values of $\Delta\xi$ in this case is quite similar to those in the case including both phase and amplitude corrections. So, we conclude that, the amplitude correction in the gravitational waveforms can only slightly influence the value $\Delta\xi$ at $m_1 \sim 12M_\odot$.

2. *Dependance on the confirmation of electromagnetic counterpart*

The coalescing binaries composed of a neutron star and a black hole could also cause the short-hard γ-ray bursts [63]. Many groups and telescopes tried to detect the electromagnetic counterparts of the GW bursts, by which one can determine the redshift of the burst. Combining the GW observation, which can determine the luminosity distance of the bursts independently, this kind of GW bursts can be treated as the standard sirens to study the expansion history of the universe [64]. Here, we should mention that once the electromagnetic counterparts of the bursts are identified, their sky-positions are also confirmed. So, the uncertainties of the position parameters (θ, ϕ) should be excluded in the determination of the parameter ξ. In order to investigate whether or not the value of $\Delta\xi$ can be significantly reduced for the sources with confirmed sky-positions, we repeat the calculation with different black-hole masses, and consider only eight free parameters $(M_c, \eta, \psi, \iota, t_c, \psi_c, d_{\rm L}, \xi)$, and plot the results of $\Delta\xi$ in Fig. 4 (the yellow dotted line). We are surprised to find that the values of $\Delta\xi$ in this case are nearly the same as those in the case with ten free parameters, which indices that cross-correlation between sky-position parameters and ξ is weak. So, we conclude that the identification of electromagnetic counterparts of GW bursts cannot significantly improve the constraint on the parameter ξ.

3. *Dependance on the sky-position, orbital and polarization angles of the sources*

Since the gravitational waveform $\tilde{h}(f)$ depends on various angles, including the sky-position angles (θ, ϕ), the inclination angle ι and the polarization angle ψ, by numerical calculations, we find that the value of $\Delta\xi$ is independent of ϕ, which is caused by the equilateral triangle structure of ET. However, the dependence of $\Delta\xi$ on the other angle parameters are quite significant. In Fig. 6, we consider the case with various angles, which shows that the value of

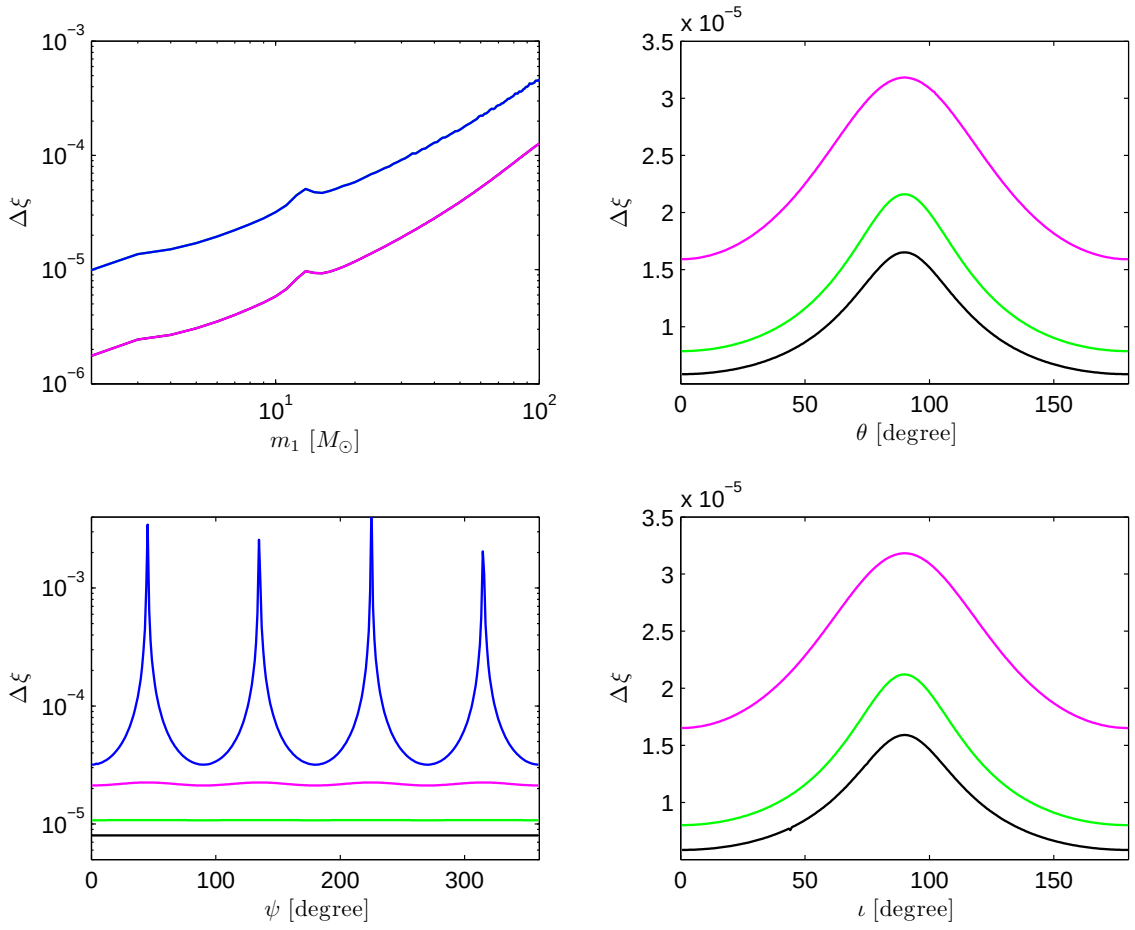

FIG. 6: **Upper left panel:** The magenta line shows the value of $\Delta\xi$ in the case with the fiducial model $\theta = \psi = \iota = 0$, and the blue line shows the result with $\theta = \psi = \iota = \pi/2$. In both cases, we have chosen $m_2 = 1.4M_\odot$, $\xi = 0$, $d_{\rm L} = 10^3$Mpc.
Upper right panel: The black, green and magenta lines show the values of $\Delta\xi$ in the cases with the fiducial model $\iota = 0$, $\iota = \pi/4$, $\iota = \pi/2$, respectively. In all cases, we have chosen $m_1 = 10M_\odot$, $m_2 = 1.4M_\odot$, $\xi = 0$, $d_{\rm L} = 10^3$Mpc, $\psi = 0$.
Lower left panel: The black, green, magenta and blue lines show the values of $\Delta\xi$ in the cases with the fiducial model $(\theta = \pi/4, \iota = 0)$, $(\theta = \pi/4, \iota = \pi/4)$, $(\theta = \pi/4, \iota = \pi/2)$, $(\theta = \pi/2, \iota = \pi/2)$, respectively. In all cases, we have chosen $m_1 = 10M_\odot$, $m_2 = 1.4M_\odot$, $\xi = 0$, $d_{\rm L} = 10^3$Mpc.
Lower right panel: The black, green and magenta lines show the values of $\Delta\xi$ in the cases with the fiducial model $\theta = 0$, $\theta = \pi/4$, $\theta = \pi/2$, respectively. In all cases, we have chosen $m_1 = 10M_\odot$, $m_2 = 1.4M_\odot$, $\xi = 0$, $d_{\rm L} = 10^3$Mpc, $\psi = 0$.

$\Delta\xi$ is minimized at $(\theta = \iota = \psi = 0)$. The dependence on θ and ι is similar, and the value of $\Delta\xi$ is maximized at $\theta = \pi/2$ and/or $\iota = \pi/2$. On the other hand, the dependence on ψ is quite different. In general, this dependence is very weak. However, in the case $\theta = \iota = \pi/2$, i.e., when the orbital plane of the binary system is coincident with the detector plane, the dependence on ψ becomes very strong. In particular, when $\psi = (1 + 2k)\pi/4$ $(k = 0, 1, 2, 3)$, it becomes very large, which is caused by the following reason: In the case with $\theta = \iota = \pi/2$ and $\psi = (1 + 2k)\pi/4$, the pattern functions of ET in Eq. (C6) are ${}_iF_+(\theta, \phi, \psi) = 0$ $(i = 1, 2, 3)$, and the cross mode in Eq. (56) is $h_\times(t) = 0$. Thus, the leading-order terms of $\tilde{h}(f)$ in Eq. (65) become zero, and the parameter constraints are quite loose in this case.

Now, let us consider the angle averaged $\Delta\xi$ for the GW bursts. If we consider the restricted PN approximation of the waveform, where all the amplitude corrections of high PN orders are discarded and only PN contributions to the phase are taken into account [65], i.e.

$$\tilde{h}(f) \simeq 2^{-1/2}\frac{M_c^{5/6}}{d_{\rm L}}\sqrt{\frac{5}{48}}\pi^{-2/3}f^{-7/6}Qe^{-i\varphi_{(2,0)}}P_{(2,0)}\Theta(2f_{\rm LSO} - f)\exp[i(2\pi f t_c - \pi/4 + 2\psi(f/2))], \tag{79}$$

TABLE I: The numerical ratio $\overline{\Delta\xi}/\Delta\xi_{\rm min}$ for different cases. The angle averaged value $\overline{\Delta\xi}$ is calculated based on 10^6 random samples for each case. In each sample, we fix the parameters in the fiducial model as: $d_{\rm L}=10^3$Mpc, $t_c=0$, $\psi_c=0$, $\xi=0.001$ $m_2=1.4M_\odot$, m_1, and randomly choose the angle parameters $(\theta,\cos\phi,\cos\iota,\psi)$ in the full parameter space.

	$m_1=2M_\odot$	$m_1=5M_\odot$	$m_1=10M_\odot$	$m_1=20M_\odot$	$m_1=50M_\odot$
$\overline{\Delta\xi}/\Delta\xi_{\rm min}$	2.498	2.482	2.450	2.325	2.151

analytical calculations show that the mean value $\overline{\Delta\xi}$ obtained by averaging the angles (θ,ψ,ι) is reduced by a factor 5/2, compared with the minimal value of $\Delta\xi_{\rm min}$ (which is achieved at $\theta=\psi=\iota=0$). However, in the terms of high PN orders in amplitude, which have not been included in the restricted PN approximation, the dependence of $\tilde{h}(f)$ on the angles (θ,ψ,ι) are quite complicated through the functions $P_{(m,n)}$ and $\varphi_{(m,n)}$ (see the expressiones of $\tilde{h}^{(k)}(f)$ in Eq. (65) and the below one). So, if taking into account the contributions of these terms, the ratio $\overline{\Delta\xi}/\Delta\xi_{\rm min}$ deviates from 5/2 in general. For given GW detector, the effects of these high PN terms become more significant for the binary system with larger mass of black hole [46], which could induce the more significant deviation of the ratio from 5/2. In order to investigate this kind of derivations, for the binary systems with different masses, we simulate the random samples to compute the values of $\overline{\Delta\xi}$ and compare with the corresponding $\Delta\xi_{\rm min}$. The results are presented in Table I. As anticipated, we find that if m_1 becomes larger, the ratio $\overline{\Delta\xi}/\Delta\xi_{\rm min}$ becomes more and more deviating from 5/2. However, this table shows that the value of ratio only slightly deviates from 5/2. This is in particular the case for $m_1<10M_\odot$. So, in general, we can roughly estimate the angle averaged $\Delta\xi$ by the relation $\overline{\Delta\xi}\sim 2.5\Delta\xi_{\rm min}$.

4. Dependance on the redshifts of the sources

The redshift z affects the gravitational waveforms by two ways: First, it changes the luminosity distance $d_{\rm L}$. A higher redshift z follows a larger $d_{\rm L}$, which makes the constraint on ξ weaker. Secondly, it changes the observed masses of the binary system, i.e. $m_i=(1+z)m_{i,\rm phys}$ $(i=1,2)$. A higher z follows a larger m_i, which also makes the constraint on ξ weaker. Combining these two effects, from Fig. 7, we find that the values of $\Delta\xi$ increase about four orders if the redshift of the GW burst changes from $z=0.05$ to $z=5$. If ET observes a burst event with $m_{1,\rm phys}=2M_\odot$ and $m_{2,\rm phys}=1.4M_\odot$ at redshift $z=0.05$, we expect to obtain a constraint $\Delta\xi\sim 10^{-6}$. If this source is located at $z=1$, the constraint becomes $\Delta\xi\sim 10^{-5}$, and the corresponding constraint on $\omega_{\rm BD}$ is $\omega_{\rm BD}\gtrsim 10^5$, which is more stringent than the current upper limit. However, if the event is at $z=5$, the constraint becomes quite loose, i.e. $\Delta\xi\sim 10^{-2}$. So, we expect that the main contribution to the constraint on ξ comes from the sources in the lowest redshift band.

For a given redshift z, we can calculate the averaged value $\langle\Delta\xi\rangle$ by taking into account the distribution of black hole masses $m_{1,\rm phys}$, and the angles (θ,ϕ,ψ,ι). Assuming the uniform distribution of $m_{1,\rm phys}$ in the range from $2M_\odot$ to $100M_\odot$, we plot the results in Fig. 8, from which we find that $\langle\Delta\xi\rangle=1.6\times10^{-5}$ for $z=0.05$, and $\langle\Delta\xi\rangle=1.1\times10^{-3}$ for $z=1$. Comparing with the results in Fig. 7, we find that for any given redshift z, the value of $\langle\Delta\xi\rangle$ is much larger than $\Delta\xi$, which is caused by the contribution of higher mass black holes when performing averaging in Fig. 8.

5. Dependance on the total number and distribution of burst events

The expected rate of coalescences per year within the horizon of ET is very large for neutron star/neutron star binaries and neutron star/black hole binaries [48]. In comparison with the case with a single GW burst event, combining all the events together can significantly improve the constraint on the parameter ξ. In this subsection, we shall focus on this issue.

For a given cosmological model, the number distribution $f(z)$ of the GW burst events is given by

$$f(z)=\frac{4\pi\mathcal{N}r(z)d_{\rm C}^2(z)}{H(z)(1+z)}, \tag{80}$$

where $d_{\rm C}$ is the comoving distance, which is defined as $d_{\rm C}(z)=\int_0^z 1/H(z')dz'$ [37]. The function $r(z)$ describes the time evolution of the burst rate, and the constant $\mathcal{N}$ (the number of the sources per comoving volume at redshift $z=0$ over the observation period) is fixed by requiring the total number of the sources $N_{\rm GW}=\int_0^{z_{\rm max}} f(z)dz$. Actually, the distribution of the events is quite unclear, since no any GW burst of this kind has been detected until now [66]. Even

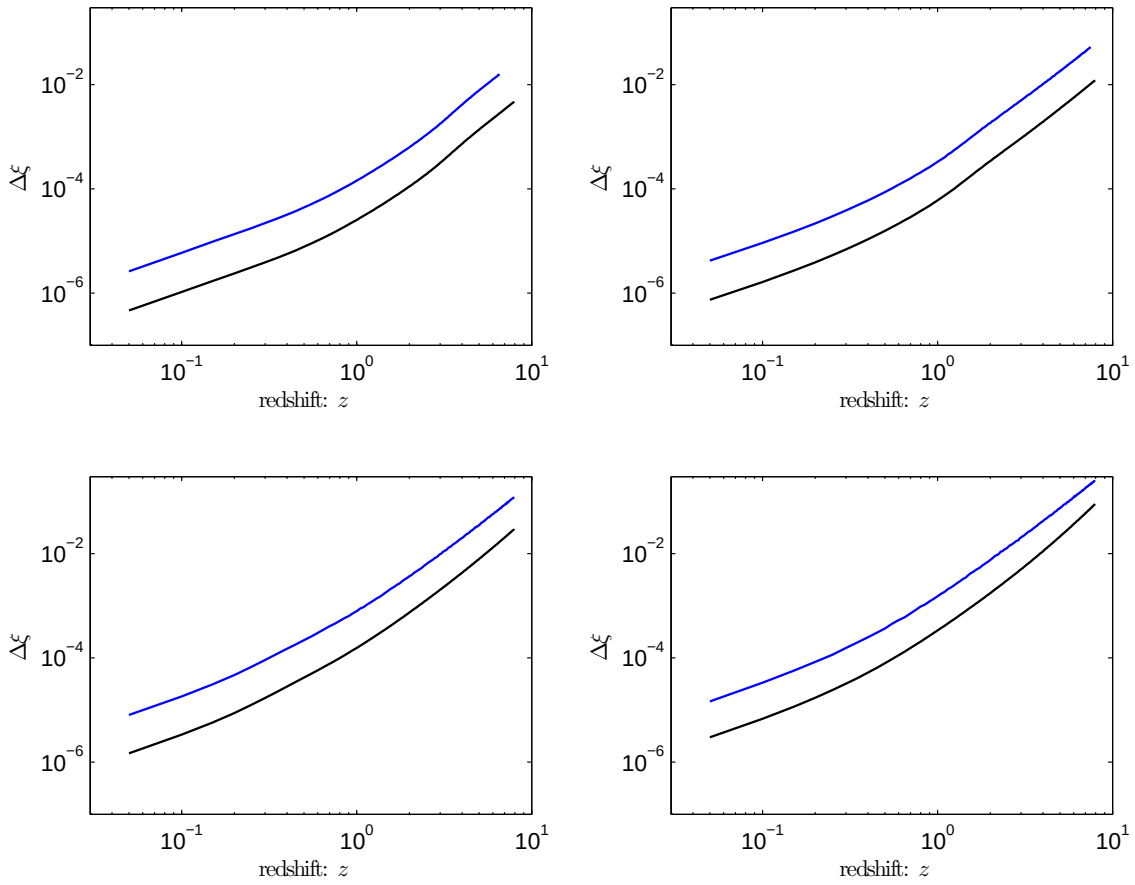

FIG. 7: The value of $\Delta\xi$ is determined by the GW bursts at different redshifts z. In the upper left panel, we consider the binary system with ($m_{1,\rm phys} = 2M_\odot$, $m_{2,\rm phys} = 1.4M_\odot$). In the upper right panel, we consider the system with ($m_{1,\rm phys} = 5M_\odot$, $m_{2,\rm phys} = 1.4M_\odot$). In the lower left panel, we consider the system with ($m_{1,\rm phys} = 10M_\odot$, $m_{2,\rm phys} = 1.4M_\odot$). In the lower right panel, we consider the system with ($m_{1,\rm phys} = 20M_\odot$, $m_{2,\rm phys} = 1.4M_\odot$). In each panel, the black line shows the results with ($\theta = \psi = \iota = 0$), and the blue line shows the results with ($\theta = \psi = \iota = \pi/2$).

for the stable orbiting systems of neutron star/black hole, this has not been confirmed from observation [67]. The theoretical estimation shows that the number of neutron star/black hole binary systems should be one or two orders smaller than those of neutron star/neutron star [68]. Since, the expected total number of inspirals per year within the horizon of ET is about several $\times 10^5$ for neutron star binaries [48], we expect that the total number of inspiraling neutron star/black hole binaries per year is $\sim 10^4$. However, two factors may increase this estimation: First, the discovery of GW bursts, GW150914 and GW151226 may imply that the number of stellar-mass black hole is larger than we expected above [69]. Second, the neutron star/black hole binaries always emit stronger GW signals, so the detectable distance of this systems is larger than that of binary neutron stars. Taking into account these factors, for ET, the number of detectable neutron star/black hole binary systems could be similar to that of neutron star/neutron star [68].

In addition to the total number, the time evolution of the source rate is also not clear. In this paper we shall consider two different forms for the function $r(z)$. In the first case we assume that the sources are distributed uniformly, i.e., with constant comoving number density throughout the redshift range $0 \leq z \leq 5$ (hereafter we will refer to this as the uniform distribution). In this case we have $r(z) = 1$. In the other case, we take $r(z)$ to be the following function: $r(z) = (1 + 2z)$ for $z \leq 1$, $r(z) = (15 - 3z)/4$ for $1 < z < 5$, and $z = 0$ for $z \geq 5$. This approximate fit to the rate evolution is suggested in [70]. Hereafter, we shall call this the nonuniform distribution. In the upper panel of Fig. 9, we plot the normalized distribution function f as a function of redshift z in the two cases. Note that in the case with the nonuniform distribution, the sources are a little bit more concentrated at $z = 1$. In what follows we will find out how this affects the uncertainties on the model parameters.

Considering multiple independent GW burst events, the combined rms error of the parameter ξ can be calculated

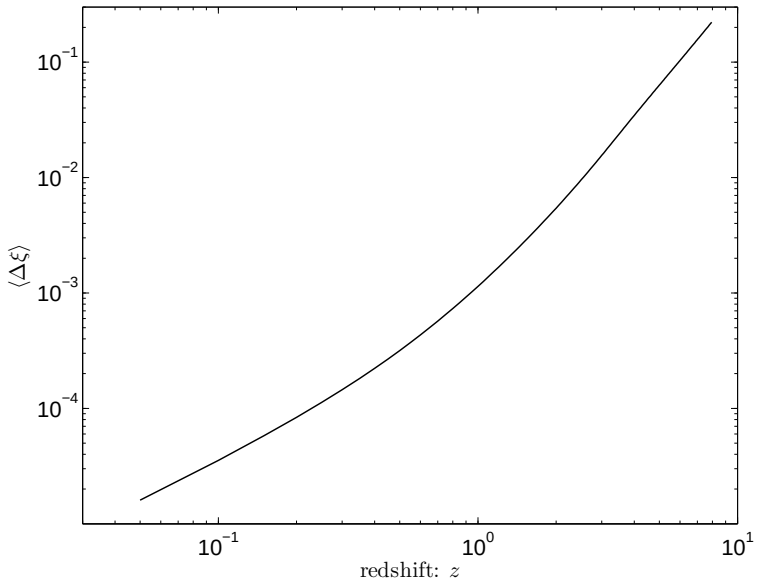

FIG. 8: The average value of $\langle\Delta\xi\rangle$ for different redshifts z. Note that, $\langle\Delta\xi\rangle$ is computed by averaging the parameters $(m_1, \theta, \psi, \iota)$, where we take $m_{1,\rm phys} \in [2, 100]M_\odot$, $\cos\theta \in [-1, 1]$, $\psi \in [0, 2\pi]$ and $\cos\iota \in [-1, 1]$. The other parameters in the fiducial model are given by $m_{2,\rm phys} = 1.4M_\odot$, $\phi = 0$, $t_c = 0$, $\psi_c = 0$ and $\xi = 0$.

by

$$[\Delta\xi]_{\rm combined} = \left(\sum_{k=1}^{N_{\rm GW}} \frac{1}{[\Delta\xi(k)]^2}\right)^{-1/2} \tag{81}$$

where $\Delta\xi(k)$ is the error of ξ derived from the k-th source. For the given normalized distribution of the sources, the value of $[\Delta\xi]_{\rm combined}$ depends on the total number $N_{\rm GW}$ through $\Delta\xi \propto 1/\sqrt{N_{\rm GW}}$. In the lower panel of Fig. 9, we plot the combined error of ξ by combining all the objects in the range $z \in [0.05, z_{\rm max}]$, where we have assumed the total number of events $N_{\rm GW} = 10^4$ at $z_{\rm max} = 5$, and the uniform distributions of the parameters $m_{1,\rm phys} \in [2, 100]M_\odot$, $\cos\theta \in [-1, 1]$, $\psi \in [0, 2\pi]$ and $\cos\iota \in [-1, 1]$. From this panel, we find that

$$[\Delta\xi]_{\rm combined} = 1.23 \times 10^{-6}\left(\frac{10^4}{N_{\rm GW}}\right)^{1/2}, \quad \text{i.e. } \omega_{\rm BD} > 0.81 \times 10^6\left(\frac{N_{\rm GW}}{10^4}\right)^{1/2}, \tag{82}$$

for the case with the uniform distribution. So, even in the conservative case with $N_{\rm GW} = 10^4$, the constraint on $\omega_{\rm BD}$ will be 20 times more stringent than the current upper limit derived from the Cassini experiment. If we consider the case $N_{\rm GW} = 2 \times 10^5$ observed by ET, the constraint of $\omega_{\rm BD}$ will be improved by two orders compared with the current upper limit. From the lower panel of Fig. 9, we also find that the main contribution comes from the events in the low frequency range, and the contribution of sources at $z > 1$ is ignorable. For the case with the nonuniform distribution, the constraint becomes

$$[\Delta\xi]_{\rm combined} = 1.37 \times 10^{-6}\left(\frac{10^4}{N_{\rm GW}}\right)^{1/2}, \quad \text{i.e. } \omega_{\rm BD} > 0.73 \times 10^6\left(\frac{N_{\rm GW}}{10^4}\right)^{1/2}, \tag{83}$$

which is slightly weaker than that in the uniform case, since in the nonuniform case, less events are distributed in the low frequency range $z < 0.5$.

IV. CONCLUSIONS

The discovery of GW bursts GW150914 and GW151226 by LIGO opens the new era of the GW astronomy, where tests of different theories of gravity in the strong gravitational fields is one of the most important issues. The

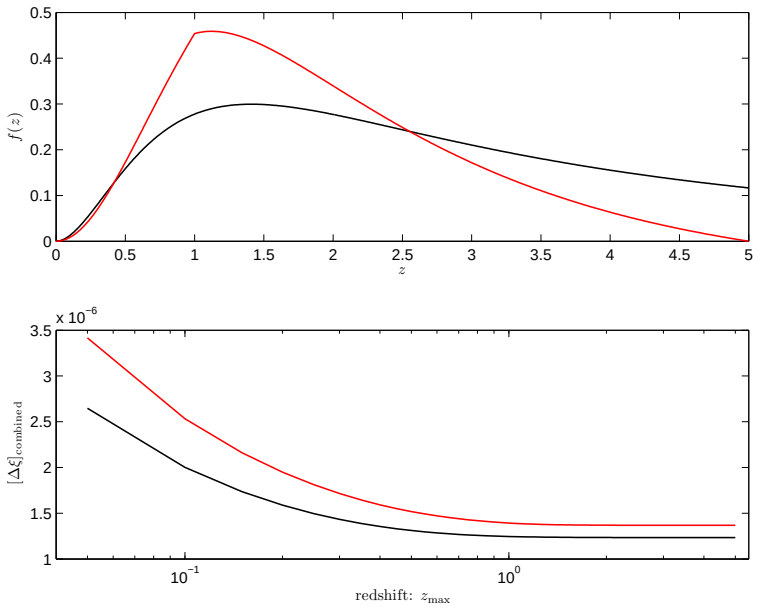

FIG. 9: **Left panel:** The normalized distribution of GW sources in the case with the uniform distribution (the black line) and the nonuniform distribution (the red line).
Right panel: The combined $[\Delta\xi]_{\rm combined}$ by considering all the objects in the redshift range $z \in [0.05, z_{\rm max}]$. In this figure, we have assumed 10^4 observed objects in the whole redshift range $z \in [0.05, 5]$. The black and red lines show the results of the uniform and nonuniform distributions of the objects, respectively.

current observations of the advanced LIGO have placed interesting constraints on some theories. By ET, a third-generation ground-based GW observatory, the total number and the distance of the observable GW sources, including the inspiralling binary systems, will be greatly improved, which will provide an excellent laboratory to precisely test various gravitational effects, as well as various theories of gravity in the strong gravitational fields. As an example, in this paper, we investigate the test ability of ET on BD gravity by constraining the model parameter $\omega_{\rm BD}$. Up to the lowest PN order, we first calculate the waveforms of gravitational radiations, including the quadrupole radiation of the metric field, and the monopole, dipole, quadrupole radiations of the scalar field, and then decompose them into the "plus", "cross" and "breathing" modes. Employing the stationary phase approximation, we derive the Fourier transforms of these modes, and parameterize the modifications of waveforms in the amplitude, phase and polarization, relative to those in GR. Utilizing the Fisher information matrix, we study the potential constraints on the parameter $\omega_{\rm BD}$ by ET, and find that an inspiralling compact binary system composed of a neutron star and a black hole gives the strongest constraints on BD gravity. The bound on $\omega_{\rm BD}$ depends on the mass of the black hole, the redshift of the system, and the sky-position angle θ, the inclination angle of binary's orbital ι and the polarization angle ψ. Consistent with the previous results, we find that the system with a lower mass can give rise to a tighter bound on $\omega_{\rm BD}$. If a binary system with a $2M_\odot$ black hole at redshift $z = 0.1$ is observed by ET, one expects to obtain a bound $\omega_{\rm BD} \gtrsim O(10^6)$, which is much more stringent than the current bound derived from the Cassini-Huygens experiment. Combining all the GW burst events can significantly improve the bound, which could arrive at $\omega_{\rm BD} \gtrsim 10^6 \times (N_{\rm GW}/10^4)^{1/2}$. So, even in the very conservative considerations with the total number of events $N_{\rm GW} = 10^4$, the bound is more than one order tighter than the current limit obtained from solar system experiments. Hence, we conclude that the testing ability of ET on theories of gravity is quite promising.

Acknowledgments

We appreciate the helpful discussion with Zhoujian Cao. W. Zhao is supported in part by NSFC Grants Nos. 11603020, 11633001, 11173021, 11322324, 11653002 and 11421303, the project of Knowledge Innovation Program of Chinese Academy of Science, the Fundamental Research Funds for the Central Universities and the Strategic Priority Research Program of the Chinese Academy of Sciences Grant No. XDB23010200. A. Wang is supported in part by Ciencia Sem Fronteiras, Grant No. A045/2013 CAPES, Brazil, and Chinese NSF, Grant Nos. 11375153 and 11173021.

Appendix A: Decomposing polarization modes of gravitational wave

A generic GW detector measures the local components of the "electric" components of the Riemann curvature tensor R^{0i0j}, which can be formally written as $R^{0i0j} \equiv -(1/2)d^2\mathrm{h}^{ij}/dt^2$. In general there are six independent components, which can be expressed in terms of polarizations [1]. For a wave propagating in the z-direction, they can be displayed as by the matrix

$$\mathrm{h}_{ij}(t) = \begin{pmatrix} h_b + h_+ & h_\times & h_x \\ h_\times & h_b - h_+ & h_y \\ h_x & h_y & h_L \end{pmatrix}. \tag{A1}$$

Three modes (h_+, $h_\times$ and h_b) are transverse to the direction of propagation, with two (h_+, $h_\times$) representing quadrupole deformations and one (h_b) representing a monopole, i.e. the breathing deformation. Three modes are longitudinal, with one (h_L) axially symmetric stretching mode in the propagation direction, and one quadrupole mode in each of the two orthogonal planes containing the propagation direction (h_x and h_y).

Now, let us turn to the GW $\mathrm{h}_{ij}(t)$ that propagates in the direction $\hat{n} = (1, \theta, \phi)$ in the coordinate system $X \equiv (x, y, z)$. We first consider the GW in another coordinate system $X' \equiv (x', y', z')$ with $\hat{n} = \hat{z}'$, where we have

$$h_+ \;=\; (\mathrm{h}'_{11} - \mathrm{h}'_{22})/2, \quad h'_\times = \mathrm{h}'_{12}, \quad h_b = (\mathrm{h}'_{11} + \mathrm{h}'_{22})/2, \quad h_L = \mathrm{h}'_{33}, \quad h_x = \mathrm{h}'_{13}, \quad h_y = \mathrm{h}'_{23}. \tag{A2}$$

The tensor h'_{ij} relates to h_{ij} by $\mathrm{h}'_{ij} = (R^T \mathrm{h} R)_{ij}$, and the transformation tensor R is given by

$$R = \begin{pmatrix} \cos\phi & \sin\phi & 0 \\ -\sin\phi & \cos\phi & 0 \\ 0 & 0 & 1 \end{pmatrix} \begin{pmatrix} 1 & 0 & 0 \\ 0 & \cos\theta & \sin\theta \\ 0 & -\sin\theta & \cos\theta \end{pmatrix}. \tag{A3}$$

Thus, we derive the following decompositions

$$\begin{aligned}
h_+ \;=\; & \frac{1}{2}\big\{\mathrm{h}_{11}(\cos^2\phi - \cos^2\theta\sin^2\phi) + \mathrm{h}_{22}(\sin^2\phi - \cos^2\phi\cos^2\theta) - \mathrm{h}_{33}\sin^2\theta \\
& - \mathrm{h}_{12}[\sin 2\phi(1+\cos^2\theta)] + \mathrm{h}_{13}\sin\phi\sin 2\theta + \mathrm{h}_{23}\cos\phi\sin 2\theta\big\}, \qquad \text{(A4)} \\
h_\times \;=\; & \frac{1}{2}\{(\mathrm{h}_{11} - \mathrm{h}_{22})\cos\theta\sin 2\phi + \mathrm{h}_{12}(2\cos\theta\cos 2\phi) - \mathrm{h}_{13}(2\sin\theta\cos\phi) + \mathrm{h}_{23}(2\sin\theta\sin\phi)\}, \qquad \text{(A5)} \\
h_b \;=\; & \frac{1}{2}\big\{\mathrm{h}_{11}(\cos^2\phi + \cos^2\theta\sin^2\phi) + \mathrm{h}_{22}(\sin^2\phi + \cos^2\phi\cos^2\theta) + \mathrm{h}_{33}\sin^2\theta \\
& - \mathrm{h}_{12}(\sin 2\phi\sin^2\theta) - \mathrm{h}_{13}\sin\phi\sin 2\theta - \mathrm{h}_{23}\cos\phi\sin 2\theta\big\}, \qquad \text{(A6)} \\
h_L \;=\; & \frac{1}{2}\big\{\mathrm{h}_{11}(2\sin^2\theta\sin^2\phi) + \mathrm{h}_{22}(2\cos^2\phi\sin^2\theta) + \mathrm{h}_{33}(2\cos^2\theta) \\
& + \mathrm{h}_{12}(2\sin 2\phi\sin^2\theta) + \mathrm{h}_{13}(2\sin\phi\sin 2\theta) + \mathrm{h}_{23}(2\cos\phi\sin 2\theta)\big\}, \qquad \text{(A7)} \\
h_x \;=\; & \frac{1}{2}\{(\mathrm{h}_{11} - \mathrm{h}_{22})\sin\theta\sin 2\phi + \mathrm{h}_{12}(2\sin\theta\cos 2\phi) + \mathrm{h}_{13}(2\cos\phi\cos\theta) \\
& - \mathrm{h}_{23}(2\sin\phi\cos\theta)\}, \qquad \text{(A8)} \\
h_y \;=\; & \frac{1}{2}\big\{\mathrm{h}_{11}(\sin 2\theta\sin^2\phi) + \mathrm{h}_{22}(\cos^2\phi\sin 2\theta) - \mathrm{h}_{33}(\sin 2\theta) \\
& + \mathrm{h}_{12}(\sin 2\phi\sin 2\theta) + \mathrm{h}_{13}(2\sin\phi\cos 2\theta) + \mathrm{h}_{23}(2\cos\phi\cos 2\theta)\big\}. \qquad \text{(A9)}
\end{aligned}$$

Appendix B: Higher post-Newtonian orders of GW waveform in Einstein's General Relativity

A compact binary system located at the sky-position (θ, ϕ) with the angle of orbital inclination ι and polarization angle ψ, including the higher PN order terms, the waveforms in the two polarizations are given by,

$$h_{+,\times}(t) = \frac{2\eta m x}{d_{\rm L}}\left\{H^{(0)}_{+,\times} + x^{1/2}H^{(1/2)}_{+,\times} + xH^{(1)}_{+,\times} + x^{3/2}H^{(3/2)}_{+,\times} + x^2H^{(2)}_{+,\times} + x^{5/2}H^{(5/2)}_{+,\times} + O(1/c^6)\right\}, \tag{B1}$$

where $m = m_1 + m_2$ is the total mass, $\eta = m_1m_2/m^2$ is the symmetric mass ratio. The PN expansion parameter is defined as $x \equiv v^2$. The coefficients $H^{(i/2)}_{+,\times}$ $(i = 0, 1, \cdots, 5)$, are linear combinations of various harmonics with prefactors

that depend on ι and η. The lowest order ones are,

$$H_{+}^{(0)} = -(1+\cos^2\iota)\cos 2\Phi(t) - (1/96)\sin^2\iota(17+\cos^2\iota), \tag{B2}$$

$$H_{\times}^{(0)} = -2\cos\iota\sin 2\Phi(t), \tag{B3}$$

$$\Phi(t) = \phi(t) - 2m\omega_s\ln(\omega_s/\omega_0), \tag{B4}$$

where ω_0 is a constant frequency that can be conveniently chosen as the entry frequency of an interferometric detector [40]. The other terms can be found in the previous work [44].

In general, we can write them as

$$H_{+,\times}^{(s)} = \sum_n \left\{ C_{+,\times}^{(n,s)}\cos[n\Phi(t)] + D_{+,\times}^{(n,s)}\sin[n\Phi(t)] \right\} \tag{B5}$$

Thus, we have

$$h(t) \equiv F_+ h_+(t) + F_\times h_\times(t) = \frac{2\mu x}{d_{\rm L}}\sum_{n,s} x^s \left\{ C^{(n,s)}\cos[n\Phi(t)] + D^{(n,s)}\sin[n\Phi(t)] \right\} \tag{B6}$$

$$= \frac{2\mu x}{d_{\rm L}}\sum_{n,s}\left\{ x^s P_{(n,s)} e^{i[n\psi+\varphi_{(n,s)}]} \right\} \tag{B7}$$

where

$$C^{(n,s)} = F_+ C_+^{(n,s)} + F_\times C_\times^{(n,s)}, \quad D^{(n,s)} = F_+ D_+^{(n,s)} + F_\times D_\times^{(n,s)}, \tag{B8}$$

$$P_{(n,s)} = \mathrm{sign}[F_+ C_+^{(n,s)} + F_\times C_\times^{(n,s)}] \left\{ [F_+ C_+^{(n,s)} + F_\times C_\times^{(n,s)}]^2 + [F_+ D_+^{(n,s)} + F_\times D_\times^{(n,s)}]^2 \right\}^{1/2}, \tag{B9}$$

$$\varphi_{(n,s)} = \tan^{-1}\left\{ -\frac{F_+ D_+^{(n,s)} + F_\times D_\times^{(n,s)}}{F_+ C_+^{(n,s)} + F_\times C_\times^{(n,s)}} \right\}. \tag{B10}$$

The Fourier components of $h(t)$ are given by

$$\tilde{h}(f) = \sum_{k=1}^{7}\tilde{h}^{(k)}(f), \tag{B11}$$

where the harmonics are explicitly presented in [46], *e.g.*, the term $\tilde{h}^{(1)}(f)$ is given by

$$\begin{aligned}\tilde{h}^{(1)}(f) = {} & \frac{M_c^{5/6}}{d_{\rm L}}\sqrt{\frac{5}{48}}\pi^{-2/3}(2f)^{-7/6}\Big\{ e^{-i\varphi_{(1,1/2)}}P_{(1,1/2)}(2\pi mf)^{1/3} \\ & + \left[e^{-i\varphi_{(1,3/2)}}P_{(1,3/2)} + e^{-i\varphi_{(1,1/2)}}P_{(1,1/2)}S_1 \right](2\pi mf) \\ & + \left[e^{-i\varphi_{(1,2)}}P_{(1,2)} + e^{-i\varphi_{(1,1/2)}}P_{(1,1/2)}S_{3/2} \right](2\pi mf)^{4/3} \\ & + \left[e^{-i\varphi_{(1,5/2)}}P_{(1,5/2)} + e^{-i\varphi_{(1,3/2)}}P_{(1,3/2)}S_1 + e^{-i\varphi_{(1,1/2)}}P_{(1,1/2)}S_2 \right](2\pi mf)^{5/3} \Big\} \\ & \times\Theta(f_{\rm LSO}-f)\exp[i(2\pi f t_c - \pi/4 + \psi(f))].\end{aligned}$$

in which

$$S_1 = \frac{1}{2}\left(\frac{743}{336}+\frac{11}{4}\eta\right),\ S_{3/2} = -2\pi,\ S_2 = \frac{7266251}{8128512}+\frac{18913}{16128}\eta+\frac{1379}{1152}\eta^2.$$

The phase function is

$$\psi(f) = -\psi_c + \frac{3}{256(2\pi M_c f)^{5/3}}\sum_{i=0}^{7}\psi_i(2\pi mf)^{i/3}, \tag{B12}$$

where

$$\begin{aligned}
\psi_0 &= 1, \quad \psi_1 = 0, \quad \psi_2 = \frac{20}{9}\left[\frac{743}{336}+\frac{11}{4}\eta\right], \quad \psi_3 = -16\pi, \quad \psi_4 = 10\left[\frac{3058673}{1016064}+\frac{5429}{1008}\eta+\frac{617}{114}\eta^2\right], \\
\psi_5 &= \pi\left[\frac{38645}{756}+\frac{38645}{252}\ln\left(f/f_{\rm LSO}\right)-\frac{65}{9}\eta\left(1+3\ln\left(f/f_{\rm LSO}\right)\right)\right], \\
\psi_6 &= \left(\frac{11583231236531}{4694215680}-\frac{640\pi^2}{3}-\frac{6846\gamma}{21}\right)+\eta\left(-\frac{15335597827}{3048192}+\frac{2255\pi^2}{12}-\frac{1760\theta}{3}+\frac{12320\lambda}{9}\right) \\
&+ \frac{76055}{1728}\eta^2-\frac{127825}{1296}\eta^3-\frac{6848}{21}\ln[4(2\pi mf)^{1/3}], \\
\psi_7 &= \pi\left(\frac{77096675}{254016}+\frac{378515}{1512}\eta-\frac{74045}{756}\eta^2\right),
\end{aligned}$$

in which $\gamma = 0.5772$ is the Euler-Mascheroni constant, $\lambda = -0.6451$ and $\theta = -1.28$.

Appendix C: Pattern functions of Einstein Telescope

A gravitational wave with a given propagation direction $\hat{\mathbf{n}}$ can be written as

$$h_{ij}(t,\mathbf{x}) = \sum_A e^A_{ij}(\hat{\mathbf{n}})\int_{-\infty}^{\infty} df\tilde{h}_A(f)e^{-2\pi if(t-\hat{\mathbf{n}}\cdot\mathbf{x})} \tag{C1}$$

where $A = +,\times,b,L,x,y$, e^A_{ij} are the polarization tensors. We take $\mathbf{x} = 0$ as the location of the detector. For a detector which is sensitive only to GWs with a reduced wavelength much larger than its size, such as resonant masses and ground-based interferometers, we have $2\pi f\hat{\mathbf{n}}\cdot\mathbf{x} \ll 1$ over the whole detector, and we can neglect the spatial dependence of $h_{ij}(t,\mathbf{x})$. So, to study the interaction of GWs with such detectors we can simply write

$$h_{ij}(t) = \sum_A e^A_{ij}(\hat{\mathbf{n}})\int_{-\infty}^{\infty} df\tilde{h}_A(f)e^{-2\pi ift} = \sum_A e^A_{ij}(\hat{\mathbf{n}})h_A(t). \tag{C2}$$

In general, the input of the GW detector has the form

$$h(t) = D^{ij}h_{ij}(t) = \sum_A D^{ij}e^A_{ij}(\hat{\mathbf{n}})h_A(t) = \sum_A F_A(\hat{\mathbf{n}})h_A(t), \tag{C3}$$

where D^{ij} is a constant tensor which depends on the detector geometry, and is known as the detector tensor. $F_A(\hat{\mathbf{n}}) \equiv D^{ij}e^A_{ij}(\hat{\mathbf{n}})$ is the detector pattern functions.

Now, let us focus on the ET. One possible set-up for ET would be a triangular tube with 10 km edges containing three interferometers with 60 degree opening angles. Consider three interferometers with 60 degree opening angles, arranged in an equilateral triangle. Let $\hat{l}_{\rm A}$ $(A = 1,2,3)$ be unit vectors tangent to the edges of the triangles as shown in Fig. 10. These can be expressed in terms of the unit vectors $(\hat{x},\hat{y},\hat{z})$ defining a Cartesian coordinate system, where $(\hat{x},\hat{y})$ are in the detector plane:

$$\hat{l}_{\rm A} = \cos(\alpha_{\rm A})\hat{x} + \sin(\alpha_{\rm A})\hat{y}, \tag{C4}$$

with $\alpha_{\rm A} = \pi/12 + (A-1)\pi/3$. The three interferometers inside the triangular tube have detector tensors

$${}_1D^{ij} = \frac{1}{2}(\hat{l}^i_1\hat{l}^j_1 - \hat{l}^i_2\hat{l}^j_2), \quad {}_2D^{ij} = \frac{1}{2}(\hat{l}^i_2\hat{l}^j_2 - \hat{l}^i_3\hat{l}^j_3), \quad {}_3D^{ij} = \frac{1}{2}(\hat{l}^i_1\hat{l}^j_1 - \hat{l}^i_3\hat{l}^j_3), \tag{C5}$$

where $i = 1,2,3$ are spatial indices.

Assume the GW source in the direction $\hat{\mathbf{n}} = (1,\theta,\phi)$ with the polarization angle ψ in the coordinate system $(\hat{x},\hat{y},\hat{z})$.

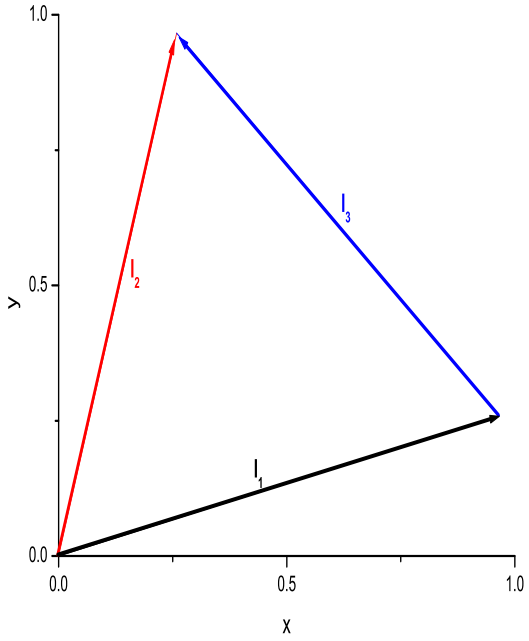

FIG. 10: Unit vectors defining the detector tensors for a triangular Einstein Telescope.

Utilizing the transformation between this system and the coordinate system $(\hat{x}', \hat{y}', \hat{z}')$, we find that

$$
\begin{aligned}
{}_1F_+(\theta,\phi,\psi) &= \frac{\sqrt{3}}{2}\left[\frac{1}{2}(1+\cos^2\theta)\cos 2\phi\cos 2\psi - \cos\theta\sin 2\phi\sin 2\psi\right], && \text{(C6)}\\
{}_1F_\times(\theta,\phi,\psi) &= \frac{\sqrt{3}}{2}\left[\frac{1}{2}(1+\cos^2\theta)\cos 2\phi\sin 2\psi + \cos\theta\sin 2\phi\cos 2\psi\right], && \text{(C7)}\\
{}_1F_b(\theta,\phi,\psi) &= \frac{\sqrt{3}}{2}\left[-\frac{1}{2}\sin^2\theta\cos 2\phi\right], && \text{(C8)}\\
{}_1F_L(\theta,\phi,\psi) &= \frac{\sqrt{3}}{2}\left[\frac{1}{2}\sin^2\theta\cos 2\phi\right], && \text{(C9)}\\
{}_1F_x(\theta,\phi,\psi) &= \frac{\sqrt{3}}{2}\left[\frac{1}{2}\sin 2\theta\cos 2\phi\cos\psi - \sin\theta\sin 2\phi\sin\psi\right], && \text{(C10)}\\
{}_1F_y(\theta,\phi,\psi) &= \frac{\sqrt{3}}{2}\left[\frac{1}{2}\sin 2\theta\cos 2\phi\sin\psi + \sin\theta\sin 2\phi\cos\psi\right], && \text{(C11)}\\
{}_2F_A(\theta,\phi,\psi) &= {}_1F_A(\theta,\phi+2\pi/3,\psi), && \text{(C12)}\\
{}_3F_A(\theta,\phi,\psi) &= {}_1F_A(\theta,\phi+4\pi/3,\psi). && \text{(C13)}
\end{aligned}
$$

[1] C. M. Will, *Theory and experiment in gravitational physics*, (Cambridge University Press, Cambridge, 1993).

[2] C. M. Will, Living Reviews in Relativity **17**, 4 (2014).
[3] T. Clifton, P. G. Ferreira, A. Padilla, and C. Skordis, Phys. Rept. **513**, 1 (2012).
[4] I. H. Stairs, Living Reviews in Relativity **6**, 5 (2003).
[5] N. Wex, *Testing Relativistic Gravity with Radio Pulsars*, to appear in the Brumberg Festschrift edited by S. M. Kopeikein (de Gruyter, Berlin, to be published) [arXiv:1402.5594].
[6] The LIGO Scientific Collaboration and the Virgo Collaboration, Phys. Rev. Lett. **116**, 061102 (2016).
[7] N. Yunes, K. Yagi and F. Pretorius, Phys. Rev. D. **94**, 084002 (2016).
[8] M. Arzano and G. Calcagni, Phys. Rev. D **93**, 124065 (2016).
[9] A. Maselli, S. Marassi, V. Ferrari, K. Kokkotas and R. Schneider, Phys. Rev. Lett. **117**, 091102 (2016).
[10] K. Popper, *The Logic of Scientific Discovery*, (MohrSiebeck, Germany, 1934).
[11] N. Yunes and F. Pretorius, Phys. Rev. D **80**, 122003 (2009); N. Loutrel, N. Yunes and F. Pretorius, Phys. Rev. D **90**, 104010 (2014).
[12] Y. Fujii and K. Maeda, *The scalar-tensor theory of gravitation*, (Cambridge University Press, Cambridge, 2003).
[13] V. Faraoni, *Cosmology in scalar-tensor gravity*, (Kluwer Academic Publishers, London, 2004).
[14] C. M. Will, Phys. Rev. D **50**, 6058 (1994).
[15] C. M. Will and H. W. Zaglauer, Astrophys. J. **346**, 366 (1989).
[16] R. N. Lang, Phys. Rev. D **89**, 084014 (2014).
[17] R. N. Lang, Phys. Rev. D **91**, 084027 (2015).
[18] S. Mirshekari and C. M. Will, Phys. Rev. D **87**, 084070 (2013).
[19] N. Sennett, S, Marsat and A. Buonanno, Phys. Rev. D **94**, 084003 (2016).
[20] T. Damour and G. Esposito-Farese, Class. Quantum Grav. **9**, 2093 (1992).
[21] J. Alsing, E. Berti, C. M. Will, and H. Zaglauer, Phys. Rev. D **85**, 064041 (2012).
[22] P. Brax, A. C. Davis, and J. Sakstein, Class. Quantum Grav. **31**, 225001 (2014).
[23] Z. Cao, P. Galaviz and L. Li, Phys. Rev. D **87**, 104029 (2013).
[24] X. Zhang, W. Zhao, H. Huang and Y. Cai, Phys. Rev. D **93**, 124003 (2016); X. Zhang, T. Liu and W. Zhao, arXiv:1702.08752.
[25] D. Bertotti, L. Iess and P. Tortota, Nature **425**, 374 (2003).
[26] P. D. Scharre and C. M. Will, Phys. Rev. D **65**, 042002 (2002).
[27] C. M. Will and N. Yunes, Class. Quantum Grav. **21**, 4367 (2004).
[28] E. Berti, A. Buonanno and C. M. Will, Phys. Rev. D **71**, 084025 (2005).
[29] K. Yagi and T. Tanaka, Phys. Rev. D **81**, 064008 (2010).
[30] K. Yagi and T. Tanaka, Prog. Theor. Phys. **123**, 1069 (2010).
[31] "The Einstein Telescope Project", `https://www.et-gw.eu/`.
[32] M. Abernathy et al., *Einstein Gravitational Wave Telescope: Conceptual Design Study,* Document No. ET-0106A-10.
[33] K. G. Arun and A. Pai, Int. J. Mod. Phys. D **22**, 1341012 (2013).
[34] E. Poisson and C. M. Will, *Gravity*, (Cambridge University Press, Cambridge, 2014).
[35] D. M. Eardley, Astrophys. J. Lett. **196**, L59 (1975).
[36] S. W. Hawking, Commun. Math. Phys. **25**, 167 (1972).
[37] S. Weinberg, *Cosmology*, (Oxford University Press, Oxford, 2008).
[38] Planck Collaboration, Astronomy and Astrophysics, **571**, A31 (2014).
[39] C. W. Misner, K. S. Thorne and J. A. Wheeler, *Gravitation*, (W. H. Freeman and Company, Newyork, 1973).
[40] M. Maggiore, *Gravitational Waves. Vol. 1: Theory and Experiments*, (Oxford University Press, Oxford, England, 2007).
[41] K. Chatziioannou, N. Yunes and N. Cornish, Phys. Rev. D **86**, 022004 (2012).
[42] C. Cutler, Phys. Rev. D **57**, 7089 (1998); M. Trias and A. M. Sintes, Phys. Rev. D **77**, 024030 (2008).
[43] L. Blanchet, Living Reviews in Relativity **5**, 3 (2002).
[44] L. Blanchet, B. R. Iyer, C. M. Will and A. G. Wiseman, Class. Quantum Grav. **13**, 575 (1996); K. G. Arun, L. Blanchet, B. R. Iyer, M. S. S. Qusailah, Class. Quantum Grav. **21**, 3771 (2004); Erratum ibid. **22**, 3115 (2005).
[45] T. Damour, P. Jaranowski, and G. Schäfer, Phys. Lett. B **513**, 147 (2001); Y. Itoh, T. Futamase, and H. Asada, Phys. Rev. D **63**, 064038 (2001); L. Blanchet, G. Faye, B. R. Iyer, and B. Joguet, Phys. Rev. D **65**, 061501(R) (2002); Erratum ibid. D **71**, 129902 (2005); Y. Itoh and T. Futamase, Phys. Rev. D **68**, 121501(R) (2003); Y. Itoh, Phys. Rev. D **69**, 064018 (2004); L. Blanchet, T. Damour, and G. Esposito-Farèse, Phys. Rev. D **69**, 124007 (2004); L. Blanchet, T. Damour, G. Esposito-Farèse, and B. R. Iyer, Phys. Rev. Lett. **93**, 091101 (2004); Y. Itoh, Class. Quantum Grav. **21**, S529 (2004); L. Blanchet and B. R. Iyer, Phys. Rev. D **71**, 024004 (2005).
[46] C. Van Den Broeck and A. S. Sengupta, Class. Quantum Grav. **24**, 155 (2007).
[47] W. Zhao, C. Van Den Broeck, D. Baskaran and T. G. F. Li, Phys. Rev. D **83**, 023005 (2011).
[48] B. S. Sathyaprakash, B. Schutz and C. Van Den Broeck, Class. Quantum Grav. **27**, 215006 (2010).
[49] S. R. Taylor and J. R. Gair, Phys. Rev. D **86**, 023502 (2012).
[50] R. Cai and T. Yang, Phys. Rev. D **95**, 044024 (2017).
[51] A. Piorkowska, M. Biesiada and Z. Zhu, JCAP **10**, 022 (2013); M. Biesiada, X. Ding, A. Piorkowska and Z. Zhu, JCAP **10**, 080 (2014); X. Ding, M. Biesiada and Z. Zhu, JCAP **12**, 006 (2015).
[52] T. Regimbau, et al., Phys. Rev. D **86**, 122001 (2012); T. Regimbau, D. Meacher and M Coughlin, Phys. Rev. D **89**, 084046 (2014); D. Meacher, K. Cannon, C. Hanna, T. Regimbau and B. S. Sathyaprakash, Phys. Rev. D **93**, 024018 (2016).
[53] J. R. Gair, I. Mandel, M. C. Miller and M. Volonteri, Gen. Rel. Grav. **43**, 485 (2011); E. A. Huerta and J. R. Gair, Phys. Rev. D **83**, 044021 (2011).

[54] B. Sathyaprakash, et al., arXiv:1108.1423; B. Sathyaprakash, et al., Class. Quantum Grav. **29**, 124013 (2012); C. Van Den Broeck, Journal of Physics: Conference Series, **484**, 012008 (2014).
[55] C. K. Mishra, K. G. Arun, B. R. Iyer and B. S. Sathyaprakash, Phys. Rev. D **82**, 064010 (2010).
[56] W. D. Pozzo, T. G. F. Li and C. Messenger, Phys. Rev. D **95**, 043502 (2017).
[57] C. Messenger and J. Read, Phys. Rev. Lett. **108**, 091101 (2012).
[58] S. Vitale and M. Evans, Phys. Rev. D **95**, 064052 (2017).
[59] X. Fan, K. Liao, M. Biesiada, A. Piorkowska-Kurpas and Z. Zhu, Phys. Rev. Lett. **118**, 091102 (2017). K. Liao, X. Fan, X. Ding, M. Biesiada and Z. Zhu, arXiv:1703.04151.
[60] A. Freise, S. Hild, K. Somiya, K. A. Strain, A. Vicere, M. Barsuglia and S. Chelkowski, Gen. Rel. Grav. **43**, 537 (2011).
[61] B. S. Sathyaprakash and B. F. Schutz, Living Reviews in Relativity **12**, 2 (2009).
[62] L. S. Finn, Phys. Rev. D **46**, 5236 (1992); L. S. Finn and D. F. Chernoff, Phys. Rev. D **47**, 2198 (1993).
[63] E. Nakar, Phys. Rept. **442**, 166 (2007).
[64] B. Schutz, Nature (London), **323**, 310 (1986).
[65] C. Cutler, et al., Phys. Rev. Lett. **70**, 2948 (1993).
[66] The LIGO Scientific Collaboration and the Virgo Collaboration, Astrophys. J. **832**, L21 (2016).
[67] J. G. Martinez, et al., Astrophys. J. **812**, 142 (2015).
[68] J. Abadie, et al., Class. Quantum Grav. **27**, 173001 (2010).
[69] The LIGO Scientific Collaboration and the Virgo Collaboration, Astrophys. J. Suppl. **227**, 14 (2016).
[70] R. Schneider, V. Ferrari, S. Matarrese and S. F. P. Zwart, Mon. Not. Roy. Astron. Soc. **324**, 797 (2001).